

Roma1 n. 978 -1993

ROM2F/93/38

Revised version (May 1994)

Deep Inelastic Scattering in Improved Lattice QCD

I. The first moment of structure functions

Stefano Capitani ¹

Giancarlo Rossi ²

¹ Dipartimento di Fisica, Università degli Studi di Roma “La Sapienza”,
and INFN, Sezione di Roma, P.le Aldo Moro 2, I-00185 Roma, Italy

² Dipartimento di Fisica, Università degli Studi di Roma “Tor Vergata”,
and INFN, Sezione di Roma 2, Via della Ricerca Scientifica, I-00133 Roma,
Italy

e-mail:

capitani@vaxrom.roma1.infn.it

rossig@vaxtov.roma2.infn.it

ABSTRACT

1 Introduction

Deep Inelastic Scattering (DIS) experiments, which started at the end of the sixties, shed light on the properties of strong interactions and on the structure of hadrons (for a comprehensive review see [1]). The study of hard processes led to the formulation of the parton model and to the hypothesis that quarks are the hadronic inner constituents [2, 3]. Further theoretical developments led to the discovery of asymptotic freedom [4, 5] and eventually to the formulation of Quantum Chromo-Dynamics [6]. Today DIS experiments are still a very important tool of investigation for short distance physics phenomena and remain the best test of QCD as a theory of strong interactions.

This paper is the first of two, focused on the computation of the renormalization constants and mixing coefficients of the operators of rank two and three that are related to the first two moments of the DIS structure functions via the Wilson operator expansion of the product of two weak or electromagnetic currents. The knowledge of the hadronic matrix elements of the Wilson operators is necessary for the theoretical evaluation of the moments of the x -distribution of quarks and gluons inside the hadrons. Our aim is to calculate to 1-loop renormalization constants and mixing coefficients of the operators related to the first and second moment in the framework of the nearest neighbor improved lattice QCD [7, 8, 9, 10]. These constants are needed to renormalize the lattice operators and be able to extract physical hadronic matrix elements from numbers obtained in Monte Carlo QCD simulations.

We present in this paper the general set up for these calculations and the results for the operators related to the first moment, leaving the discussion and the presentation of the results for the operator related to the second moment to a forthcoming paper [11]. There are two main reasons for the subdivision of the whole material in this way. One is that new high-statistics

Monte Carlo data for the first moment of DIS structure functions, produced in simulations employing the improved lattice QCD action, will soon be available. The second reason, not unrelated with the previous one, is that, since simulations concerning the second moment have been given lower priority, it has not been yet decided what precise lattice expression for the corresponding rank three operator will be finally taken. This is not immaterial from our point of view: the perturbative calculation of the renormalization constants of the rank three operators are barely within the reach of algebraic manipulation programs such as Schoonschip or Form, because of the fantastically large number of terms generated in the course of the calculation.

Renormalization constants and mixing coefficients of the rank two operators have already been calculated some time ago using the standard Wilson action with not completely consistent numerical results [12, 13, 14, 15, 16, 17]. In this work, beside checking previous calculations, we present the results obtained for these constants by using the nearest neighbor improved QCD action (also known as the “clover-leaf” action), according to the improvement program started by Symanzik in ref. [18].

The use of this action has been proven [7, 8, 9, 10] to remove from on-shell hadronic matrix elements all terms that in the continuum limit are effectively of order a , a being the lattice spacing. Recent Monte Carlo simulations [19, 20] show indeed a substantial reduction of the systematic errors related to the finiteness of the lattice spacing, though at the price of a slightly higher theoretical and numerical computational effort.

Because of the great number of diagrams and of the complexity of the algebraic expressions involved in the calculation even in the case of the rank two operators, it has been considered necessary in this work to check all the results obtained by hand by means of suitable algebraic manipulation programs.

The computation has also taken into account internal fermion loops, hoping that the increasing power of dedicated computers would soon allow for fully unquenched QCD simulations.

We have found discrepancies at the non-improved level, that is at the level of the standard Wilson action, with some of the numbers already published in the literature [12, 13, 14, 15]. They have both numerical and analytic origin. On the other hand, we are in complete agreement with the results of refs. [16] and [17] concerning the energy-momentum tensor.

This paper is organized as follows: in Sect. 2 we discuss the general setting of the physical problem, and we immediately give the results for the renormalization constants and mixing coefficients of the relevant operators in a “ready-to-use” way. In Sect. 3 we present a brief introduction to the subject of improved lattice perturbation theory. In Sect. 4 the properties of the operators and their choice are discussed, in Sect. 5 we spell out all the necessary renormalization conditions, in Sects. 6 and 7 some peculiar aspects of the analytic and numerical calculations are explained, in Sect. 8 we present the detailed results of our computation with a comparison with previous results, and in Sect. 9 we present some conclusions and an outlook of future lines of investigations. Some of the more technical aspects of the calculations can be found in the appendices A, B, C and D.

2 General setting and results

2.1 Moments of structure functions

The DIS cross section is dominated by the field behavior in the light-like region. The expansion of the product of, for instance, two scalar field operators on the light cone has the general expression [21]

$$A(x)B(0) \sim \sum_{N,i} c_{N,i}(x^2) x^{\mu_1} \dots x^{\mu_N} O_{\mu_1 \dots \mu_N}^{(N,i)}(0), \quad (1)$$

where the $O_{\mu_1 \dots \mu_N}^{(N,i)}$ are symmetric traceless tensors with vanishing vacuum expectation value: $\langle 0 | O_{\mu_1 \dots \mu_N}^{(N,i)} | 0 \rangle = 0$. The singularity of the coefficient functions is, up to logarithms, given by

$$c_{N,i}(x^2) \sim (x^2)^{\frac{d_{O(N,i)} - N - d_A - d_B}{2}} \quad (2)$$

and is governed by the twist [22],

$$\tau = d_{O(N,i)} - N, \quad (3)$$

of the operator, that is, by the difference between its physical dimension and the spin. The lowest twist operators are thus the dominant ones.

In QCD the lowest twist operators appearing in the light-cone expansion of the product of two hadronic weak currents, relevant to DIS, are [23, 24, 25, 26, 12]

$$\begin{aligned} O_{\mu_1 \dots \mu_N}^{qS} &= \frac{1}{2^N} \bar{\psi} \gamma_{[\mu_1} \overleftrightarrow{D}_{\mu_2} \dots \overleftrightarrow{D}_{\mu_N]} (1 \pm \gamma_5) \psi \\ O_{\mu_1 \dots \mu_N}^{qNS} &= \frac{1}{2^N} \bar{\psi} \gamma_{[\mu_1} \overleftrightarrow{D}_{\mu_2} \dots \overleftrightarrow{D}_{\mu_N]} (1 \pm \gamma_5) \frac{\lambda^f}{2} \psi \\ O_{\mu_1 \dots \mu_N}^{gS} &= \sum_{\rho} \text{Tr} \left[F_{[\mu_1 \rho} \overleftrightarrow{D}_{\mu_2} \dots \overleftrightarrow{D}_{\mu_{N-1}} F_{\rho \mu_N]} \right], \end{aligned} \quad (4)$$

where the λ^f 's are flavor matrices. The operators (4) are gauge invariant and all have $\tau = 2$; from now on we implicitly assume that they are symmetrized

with respect to all Lorentz indices. S and NS superscripts refer to Singlet and Non Singlet flavor structures.

In the unpolarized cross section the γ_5 contributions average to zero. The other contributions have matrix elements of the form

$$\langle p | O_{\mu_1 \dots \mu_N}^{(N)} | p \rangle = A_N(\mu) p_{\mu_1} \dots p_{\mu_N} + \text{trace terms}, \quad (5)$$

where μ is the subtraction point. They contain long distance non-perturbative physics, and are related to the general expression of the moments of structure functions by the equations [27]

$$\int d\mathbf{x} x^{N-1} \mathcal{F}_k(q^2, \mathbf{x}) = C_N(q^2/\mu^2) A_N(\mu), \quad (6)$$

where we have put

$$\begin{aligned} \mathcal{F}_1 &= 2F_1 \\ \mathcal{F}_2 &= \frac{F_2}{x} \\ \mathcal{F}_3 &= F_3, \end{aligned} \quad (7)$$

with F_1 , F_2 and F_3 the usual DIS structure functions as defined in [1]. The Fourier transforms, C_N , of the Wilson coefficient functions are determined by the short distance perturbative behavior of QCD and are formally given by

$$C_N(q^2) = (q^2)^N \left(\frac{\partial^2}{\partial q^2} \right)^N \int d^4x e^{iqx} c_N(x^2). \quad (8)$$

When renormalization effects are taken into account, a dependence upon the subtraction point μ appears in both sides of eq. (8).

The C_N 's are perturbatively calculable with renormalization group techniques. In case of mixing among different operators the Wilson coefficients satisfy a system of Callan-Symanzik equations

$$\left(\mu \frac{d}{d\mu} + \beta(g) \frac{d}{dg} \right) C_{N,l} = \sum_k (\gamma_N(g))_{lk} C_{N,k}, \quad (9)$$

where the anomalous dimensions, γ_N , have been arranged in a matrix

$$(\gamma_N)_{lk} = \mu \frac{d}{d\mu} \log(Z_N)_{lk}^{-1}. \quad (10)$$

Renormalization constants and mixing coefficients, $(Z_N)_{lk}$, are defined by suitable sets of renormalization conditions, allowing the construction of finite renormalized operators:

$$\widehat{O}^{(N,l)}(\mu) = \sum_k (Z_N(\mu))_{lk} O^{(N,k)}. \quad (11)$$

Equations (9) can be decoupled by diagonalizing the anomalous dimension matrix, so to have a new basis of operators that are multiplicatively renormalizable.

2.2 A summary of the results

We have carried out, in the chiral limit, the 1-loop perturbative lattice calculation of the renormalization constants and mixing coefficients of the following rank two operators:

$$O_{\mu\nu}^q = \frac{1}{4} \bar{\psi} \gamma_{[\mu} \overleftrightarrow{D}_{\nu]} \psi, \quad (12)$$

which is related to the first moment of the x-distribution of quarks, and

$$O_{\mu\nu}^g = \sum_{\rho} \text{Tr} [F_{\mu\rho} F_{\rho\nu}], \quad (13)$$

which is related to the first moment of the x-distribution of gluons¹. The lattice expression of $F_{\mu\nu}$ is given by

$$F_{n,\mu\nu} = \frac{1}{8ig_0a^2} \sum_{\mu\nu=\pm} (U_{n,\mu\nu} - U_{n,\mu\nu}^+), \quad (15)$$

¹We are presently computing the renormalization constant of the operator

$$O_{\mu\nu\tau}^q = \frac{1}{8} \bar{\psi} \gamma_{[\mu} \overleftrightarrow{D}_{\nu} \overleftrightarrow{D}_{\tau]} \psi, \quad (14)$$

which is connected to the second moment of the x-distribution of quarks [11].

where $U_{n,\mu\nu}$ is the usual plaquette

$$U_{n,\mu\nu} = U_{n,\mu}U_{n+\mu,\nu}U_{n+\nu,\mu}^+U_{n,\nu}^+. \quad (16)$$

The operators (12) and (13) are the first ones in the list given above in eqs. (4).

In the flavor Singlet sector, given the operators (12) and (13), the finite operators $\hat{O}_{\mu\nu}^1$ and $\hat{O}_{\mu\nu}^2$, with well defined anomalous dimensions, that are renormalized to their tree level values at $p^2 = \mu^2$ ($\mu a \ll 1$), are given to 1-loop in the full (unquenched) theory by the formulae (see Sects. 5 and 8 for details)

$$\hat{O}_{\mu\nu}^1 = \left[1 - \frac{\alpha_S}{4\pi} (N_c B_{gg} + N_f (B_{gg}^f - B_{qq})) \right] O_{\mu\nu}^g - \left[1 + \frac{\alpha_S}{4\pi} C_F (B_{gq} - B_{qq}) \right] O_{\mu\nu}^q \quad (17)$$

and

$$\begin{aligned} \hat{O}_{\mu\nu}^2 &= \left[1 - \frac{\alpha_S}{4\pi} (\gamma_2 \log \mu a + C_F B_{qq} + \frac{1}{4} N_f B_{gq}) \right] O_{\mu\nu}^q \\ &+ \frac{N_f}{4C_F} \left[1 - \frac{\alpha_S}{4\pi} (\gamma_2 \log \mu a + 4C_F B_{gq} + N_c B_{gg} + N_f B_{gg}^f) \right] O_{\mu\nu}^g, \end{aligned} \quad (18)$$

where N_c and N_f are respectively the number of colors and the number of flavors, and

$$\begin{aligned} \gamma_2 &= \frac{16}{3} C_F + \frac{4}{3} N_f \\ C_F &= (N_c^2 - 1)/2N_c \\ \alpha_S &= g_0^2/4\pi. \end{aligned} \quad (19)$$

The coefficients B for the case of the standard Wilson action and of the nearest neighbor improved action are reported (for $r = 1$) in Table 2.1. They can be derived from the more detailed Tables presented in Sect. 8. In Table

Wilson		Improved	
B_{qq}^W	-3.165	B_{qq}^I	-15.816
B_{qg}^W	0.019	B_{qg}^I	-1.041
B_{gq}^W	-5.817	B_{gq}^I	-4.044
$(B_{gg}^f)^W$	-2.168	$(B_{gg}^f)^I$	-19.425
$B_{gg} = -15.585$			

Table 2.1 - Values of the constants B on the lattice for $r = 1$

B_{qq}	sails	-4
	vertex	8/9
	self-energy	-1
	total	- 37/9
B_{qg}		- 7/9
B_{gq}		- 23/9
B_{gg}		11/12
B_{gg}^f		- 23/18

Table 2.2 - Values of the constants B in \overline{MS} regularization

2.2 we report for completeness the values of the constants B in the continuum, computed in the \overline{MS} renormalization scheme [26, 15].

In the quenched approximation one has to put $N_f = 0$ in the above formulae. Numerically, in terms of $\beta \equiv 2N_c/g_0^2$, for $N_c = 3$ one gets

- in the flavor Singlet sector

i) for the Wilson action:

$$\begin{aligned}\hat{O}_{\mu\nu}^1 &= \left[1 - \frac{9}{8\pi^2\beta}B_{gg}\right]O_{\mu\nu}^g - \left[1 + \frac{1}{2\pi^2\beta}(B_{gq}^W - B_{qq}^W)\right]O_{\mu\nu}^q \quad (20) \\ &= \left[1 + \frac{1.776}{\beta}\right]O_{\mu\nu}^g - \left[1 - \frac{0.134}{\beta}\right]O_{\mu\nu}^q\end{aligned}$$

and

$$\begin{aligned}\hat{O}_{\mu\nu}^2 &= \left[1 - \frac{8}{3\pi^2\beta}\log \mu a - \frac{1}{2\pi^2\beta}B_{qq}^W\right]O_{\mu\nu}^q \quad (21) \\ &= \left[1 - \frac{0.270}{\beta}\log \mu a + \frac{0.160}{\beta}\right]O_{\mu\nu}^q;\end{aligned}$$

ii) for the nearest neighbor improved action:

$$\begin{aligned}(\hat{O}_{\mu\nu}^1)^{IMPR} &= \left[1 - \frac{9}{8\pi^2\beta}B_{gg}\right]O_{\mu\nu}^g - \left[1 + \frac{1}{2\pi^2\beta}(B_{gq}^I - B_{qq}^I)\right](O_{\mu\nu}^q)^{IMPR} \quad (22) \\ &= \left[1 + \frac{1.776}{\beta}\right]O_{\mu\nu}^g - \left[1 + \frac{0.596}{\beta}\right](O_{\mu\nu}^q)^{IMPR}\end{aligned}$$

and

$$\begin{aligned}(\hat{O}_{\mu\nu}^2)^{IMPR} &= \left[1 - \frac{8}{3\pi^2\beta}\log \mu a - \frac{1}{2\pi^2\beta}B_{qq}^I\right](O_{\mu\nu}^q)^{IMPR} \quad (23) \\ &= \left[1 - \frac{0.270}{\beta}\log \mu a + \frac{0.801}{\beta}\right](O_{\mu\nu}^q)^{IMPR},\end{aligned}$$

where the explicit expression of $(O_{\mu\nu}^q)^{IMPR}$ can be found in eq. (50) of Sect. 6.

- For the flavor Non Singlet operator

$$O_{\mu\nu}^{fq} = \frac{1}{4} \bar{\psi} \gamma_{[\mu} \overleftrightarrow{D}_{\nu]} \frac{\lambda^f}{2} \psi \quad (24)$$

there is no mixing between O^q and O^g , and one gets

$$\hat{O}_{\mu\nu}^{fq} = \left[1 - \frac{8}{3\pi^2\beta} \log \mu a - \frac{1}{2\pi^2\beta} B_{qq} \right] O_{\mu\nu}^{fq}, \quad (25)$$

with obvious adjustments in notations in going from the Wilson to the improved case and with B_{qq} given in Table 2.1.

3 Improved lattice QCD

Lattice QCD represents today the only viable way of evaluating from first principles the matrix elements (5), needed for the computation of A_N and, hence, of the moments of the structure functions.

In this section we wish to briefly describe the improvement program of lattice QCD, as discussed in refs. [18, 28, 7, 8, 9, 10].

The QCD Wilson action for one flavor f is, on a euclidean lattice [29],

$$\begin{aligned} S_{LATT}^f = a^4 \sum_n & \left[-\frac{1}{2a} \sum_{\mu} \left[\bar{\psi}_n(r - \gamma_{\mu}) U_{n,\mu} \psi_{n+\mu} \right. \right. \\ & \left. \left. + \bar{\psi}_{n+\mu}(r + \gamma_{\mu}) U_{n,\mu}^+ \psi_n \right] + \bar{\psi}_n \left(m_f + \frac{4r}{a} \right) \psi_n \right] \\ & - \frac{1}{g_0^2} \sum_{n,\mu\nu} \left[\text{Tr} \left[U_{n,\mu} U_{n+\mu,\nu} U_{n+\nu,\mu}^+ U_{n,\nu}^+ \right] - N_c \right]. \end{aligned} \quad (26)$$

The gauge field $A_{n,\mu}$ is introduced through the definition

$$U_{n,\mu} = e^{ig_0 a t^A A_{n,\mu}^A} \quad (A = 1, \dots, N_c^2 - 1). \quad (27)$$

Fermion fields are site variables, while the $U_{n,\mu}$'s are link variables. $U_{n,\mu}$ is associated to the link connecting the site n with the site $n + \mu$. From

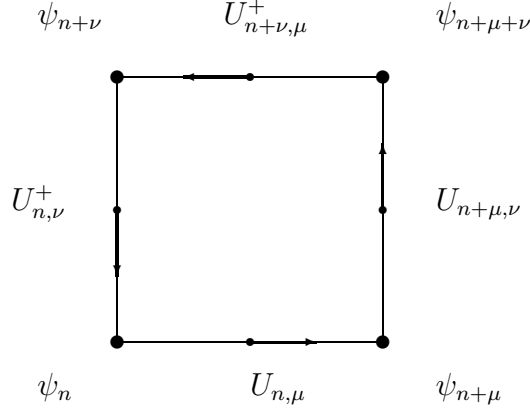


Fig. 1 - The $\mu\nu$ -plaquette in lattice QCD

this action one can derive the Feynman rules for lattice perturbation theory. Conventionally $A_{n,\mu}$ will be taken to sit at the point $n + \mu/2$, the middle point of the link $(n, n + \mu)$ (see Fig. 1). This choice greatly simplifies Feynman rules.

The computations of physical quantities with Monte Carlo simulations are affected by statistical and systematic errors. The one which we are mainly concerned with here is the systematic error due to the finiteness of the lattice spacing. In fact for a renormalized finite lattice operator, $\widehat{\mathcal{O}}_L$, we have the formal expansion

$$\langle p | \widehat{\mathcal{O}}_L | p' \rangle_{Monte\ Carlo} = a^d \left[\langle p | \widehat{\mathcal{O}} | p' \rangle_{phys.} + O(a) \right], \quad (28)$$

where $\langle p | \widehat{\mathcal{O}} | p' \rangle_{phys.}$ is the physical matrix element we want to extract from Monte Carlo data and d is its physical dimension. We see from equation (28) that the possibility of estimating $\langle p | \widehat{\mathcal{O}} | p' \rangle_{phys.}$ from Monte Carlo simulations depends on the magnitude of $O(a)$ terms, which is generally between 20 and 30 percent. The effect of improvement is the removal of all corrections that

in the continuum limit ($g_0^2 \sim 1/\log a$) are effectively of order a , that is to say, of all terms that in perturbation theory are of the type

$$a(g_0^2)^n(\log a)^n \sim "a". \quad (29)$$

This result is achieved through the addition of “irrelevant” interaction terms to the Wilson action and by adjusting (“improving”) the lattice expression of fermion operators, so as to cancel unwanted contributions in their matrix elements [18], thus making faster the recovery of the continuum properties in the limit $a \rightarrow 0$. It is estimated that with this method one can achieve a reduction of the systematic error due to the finiteness of the lattice spacing down to 5 - 10 percent [19, 20].

The first proposal of improvement of the fermionic part of the QCD action presented, however, the drawback of having next-to-nearest neighbor interactions [30, 31, 32]. This feature is a problem in Monte Carlo simulations, given the calculational effort required for the numerical inversion of the fermion propagator (to date the only simulation carried out with the next-to-nearest neighbor improved action is that of ref. [33]). A great step forward was made by Lüscher and Weisz, who introduced the notion of on-shell improvement [28]: on-shell improvement is a weaker requirement than full improvement and easier to implement. Immediately after, Sheikholeslami and Wohlert [7] proposed the nearest neighbor fermion action employed today and started the study of its properties. In ref. [8] the relation between the Sheikholeslami-Wohlert action and the next-to-nearest action was elucidated and it was shown that the Sheikholeslami-Wohlert action leads to on-shell improvement, with the consequence that all spectral quantities are free from terms that in the continuum limit are effectively of order “ a ” (eq. (29)), provided that hadronic operators are at the same time appropriately “improved”.

The developments of these researches on on-shell improvement led to a practical recipe for its application to QCD [8, 9, 10]. This consists in modifying the standard Wilson action by adding the nearest-neighbor interaction term

$$\Delta S_I^f = -ig_0 a^4 \sum_{n,\mu\nu} \frac{r}{4a} \bar{\psi}_n \sigma_{\mu\nu} F_{n,\mu\nu} \psi_n. \quad (30)$$

Here $F_{n,\mu\nu}$ is not the naive lattice “plaquette”

$$P_{n,\mu\nu} = \frac{1}{2ig_0 a^2} (U_{n,\mu\nu} - U_{n,\mu\nu}^+) \quad (31)$$

$$U_{n,\mu\nu} = U_{n,\mu} U_{n+\mu,\nu} U_{n+\nu,\mu}^+ U_{n,\nu}^+,$$

but rather the average of the four plaquettes lying in the plane $\mu\nu$, stemming from the point n :

$$F_{n,\mu\nu} = \frac{1}{4} \sum_{\mu\nu=\pm} P_{n,\mu\nu} = \frac{1}{8ig_0 a^2} \sum_{\mu\nu=\pm} (U_{n,\mu\nu} - U_{n,\mu\nu}^+). \quad (32)$$

Because of the form of $F_{n,\mu\nu}$, the Sheikholeslami-Wohlert action is often referred to as the “clover-leaf” action.

The term (30), because of the antisymmetry of $\sigma_{\mu\nu}$ matrices, does not alter the quark-gluon interactions with an even number of gluons. The interactions with an odd number of gluons are on the contrary modified. For 1-loop calculations this results in the appearance of the new vertex

$$(V^I)_\rho^{bc}(k, k') = -g_0 \frac{r}{2} (t^A)_{bc} \cos \frac{a(k - k')_\rho}{2} \sum_\lambda \sigma_{\rho\lambda} \sin a(k - k')_\lambda, \quad (33)$$

where k and k' are the momenta of the incoming and of the outgoing fermions, and ρ is the Lorentz index carried by the gluon, to be added to the standard Wilson vertex

$$(V)_\rho^{bc}(k, k') = -g_0 (t^A)_{bc} \left[r \sin \frac{a(k + k')_\rho}{2} + i\gamma_\rho \cos \frac{a(k + k')_\rho}{2} \right]. \quad (34)$$

Besides this modification of the action, in the calculation of an n -point fermion Green function, one has to perform on each fermion field the rotation (see appendix A for the definition of the lattice covariant derivatives)

$$\begin{aligned}\psi &\longrightarrow \left(1 - \frac{ar}{2} \overrightarrow{\mathcal{D}}\right) \psi \\ \bar{\psi} &\longrightarrow \bar{\psi} \left(1 + \frac{ar}{2} \overleftarrow{\mathcal{D}}\right).\end{aligned}\tag{35}$$

As we said, it was proven in ref. [8] that this recipe allows to get rid in on-shell matrix elements of all terms that in perturbation theory are of the form (29). The removal of these leading log terms leaves us with next-to-leading terms of the kind

$$a(g_0^2)^n \log^{n-1} a,\tag{36}$$

which are effectively of order “ $a/\log a$ ”. The improvement recipe thus lowers the difference between continuum and lattice from (28) to

$$\langle p | \widehat{\mathcal{O}}_L | p' \rangle_{Monte\ Carlo}^{IMPR.} = a^d \left[\langle p | \widehat{\mathcal{O}} | p' \rangle_{phys.} + O(a/\log a) \right].\tag{37}$$

Getting rid of also the next-to-leading terms would require a bunch of 1-loop computations. They are necessary to adjust to next order the coefficient in front of eq. (30) and the form of the transformation (35). A crucial step forward in this direction has been carried out in ref. [34] where the g_0^2 correction to the factor in front of eq. (30) has been computed. This is enough to improve to next-to-leading log’s the values of the hadron masses measured in Monte Carlo simulations [35, 36].

4 The operators

We have computed, in the chiral limit, the four forward matrix elements

$$\begin{pmatrix} \langle q | O_{\mu\nu}^q | q \rangle & \langle g, \sigma | O_{\mu\nu}^q | g, \sigma \rangle \\ \langle q | O_{\mu\nu}^g | q \rangle & \langle g, \sigma | O_{\mu\nu}^g | g, \sigma \rangle \end{pmatrix},\tag{38}$$

where $|q\rangle$ is a one-quark state of momentum p and vanishing (renormalized) mass and $|g, \sigma\rangle$ is a one-gluon state of momentum p and polarization σ .

It should be noticed that beyond tree level there will be in general a mixing in the flavor Singlet sector between the quark operator O^q and the gluon operator O^g . However, in the “quenched” approximation ($N_f = \text{number of flavors} = 0$) one has $\langle g, \sigma | O_{\mu\nu}^q | g, \sigma \rangle = 0$. In this case the matrix (38) becomes triangular and the operator O^q will not mix anymore with O^g (see eqs. (47), (48) and (49) below).

To write the operators (12) and (13) in a euclidean lattice, we need to take into account the changes in the symmetry properties of the Lagrangian [37, 38] due to the the breaking of the euclidean Lorentz group $O(4)$ down to the discrete hypercubic group $H(4)$:

$$O(4) \longrightarrow H(4) \tag{39}$$

(continuum \rightarrow cubic lattice).

The hypercubic group $H(4)$ is the group of the discrete rotations of the lattice onto itself. It is a finite subgroup of the ortogonal four dimensional group $O(4)$, consisting of 192 elements. $H(4)$ admits 13 irreducible representations.

The breaking (39) implies that the operators belonging to irreducible representations of $O(4)$ may transform in a reducible way under $H(4)$, thus inducing a mixing under renormalization among operators belonging to different irreducible $O(4)$ representations. This mixing adds to the mixing between (12) and (13), and causes further complications in the computation, even if the new operators have the same dimensions as the original one. If they have lower dimensions the coefficient of the mixing will inevitably contain negative powers of a , giving rise to power divergences: they can only be subtracted from the original operator in a non-perturbative way [39].

To avoid all these unwanted mixings we need to choose particular values of the $\mu\nu$ -indices in eqs. (12) and (13), together with an appropriate lattice expression for the gauge field strength, $F_{\mu\nu}$, in eq. (13).

First, we note that actually the quark operator has the explicit form

$$O_{\mu\nu}^q = \frac{1}{4} \bar{\psi} \gamma_{[\mu} \overleftrightarrow{D}_{\nu]} \psi - \delta_{\mu\nu} \cdot \text{tr}, \quad (40)$$

and the like for the gluon case (13). The subtraction of trace terms, symbolically indicated by “tr” in eq. (40), reduces eq. (5) to the simpler form

$$\langle p | O_{\mu_1 \dots \mu_N}^{(N)} | p \rangle = A_N p_{\mu_1} \dots p_{\mu_N}. \quad (41)$$

The operator $O_{\mu\nu}^q$ with no trace subtraction is the sum of two irreducible representations of H(4): a four-dimensional one, corresponding to $\mu = \nu$, and a six-dimensional one, corresponding to $\mu \neq \nu$. With the subtraction of the trace the singlet is removed from the four-dimensional representation, which therefore becomes three-dimensional and cannot mix any more with the dangerous lower dimensional singlet operator $\bar{\psi} \psi$ with a linearly divergent coefficient. However, large errors would result when the subtraction of the trace contribution is numerically performed on Monte Carlo data. The other option is therefore to choose $\mu \neq \nu$. As we said above, this leads to an irreducible H(4) representation, so there will be no mixing with other operators. With this choice it will be necessary to give the hadron a momentum different from zero in one of the two μ or ν directions. This causes a somewhat stronger sensitivity of Monte Carlo data to the granularity of the lattice.

In actual Monte Carlo simulations [13, 14] the choice $\mu \neq \nu$ has always been made, as the magnitude of the systematic errors associated with it is smaller than the one coming from the numerical subtraction of the trace contribution. In this paper also we will work with $\mu \neq \nu$. This, by the way, induces remarkable simplifications in the calculations.

We further restricted ourselves to the chiral case, that is to the case in which the (renormalized) quark mass is zero. This choice corresponds to the limiting situation of vanishing pion mass, to which Monte Carlo data are always extrapolated.

As for the gluon operator, the same lattice approximation of the gluon field strength that is chosen in (32) turns out to avoid mixing of O^g with undesired operators [37, 38]. In fact the operator (31) transforms like a 24-dimensional reducible representation and the product $P_{\mu\rho} \cdot P_{\rho\nu}$, with $\mu \neq \nu$, transforms like a 192-dimensional reducible representation. In particular $P_{\mu\rho} \cdot P_{\rho\nu}$ mixes with the operator $\bar{\psi}\psi$ with a power divergent coefficient. On the contrary, with the definition (32), which maximizes the symmetry of the expression of the field strength on the lattice, $F_{n,\mu\nu}$ will transform like the direct sum of two three-dimensional irreducible representations corresponding to the two combinations $E + B$ and $E - B$. Also in this case we choose $\mu \neq \nu$ to avoid the need for trace subtraction.

5 Renormalization conditions

The renormalization conditions connect the bare lattice operators on the lattice to finite operators renormalized at a scale μ :

$$\widehat{O}^l(\mu) = Z_{lk}(\mu a) O^k(a). \quad (42)$$

The constants Z_{lk} are fixed in perturbation theory by the same renormalization conditions used in the continuum. As we have discussed in the previous section, in the flavor Singlet case there is a mixing between the quark and gluon operators (12) and (13) that have the same conserved quantum numbers. However, with the choice $\mu \neq \nu$ and the definition (32) of the gauge field strength we avoid mixing with other operators of possibly lower dimensions, and therefore the need for subtraction of power divergences.

We thus write:

$$\begin{aligned}\widehat{O}^q &= Z_{qq}O^q + Z_{qg}O^g \\ \widehat{O}^g &= Z_{gq}O^q + Z_{gg}O^g,\end{aligned}\tag{43}$$

where the Z 's are determined by imposing the renormalization conditions:

$$\begin{aligned}\langle q|\widehat{O}^q(\mu)|q\rangle &= \langle q|O^q(a)|q\rangle \Big|_{p^2=\mu^2}^{tree} \\ \langle g,\sigma|\widehat{O}^q(\mu)|g,\sigma\rangle &= \langle g,\sigma|O^q(a)|g,\sigma\rangle \Big|_{p^2=\mu^2}^{tree} = 0 \\ \langle q|\widehat{O}^g(\mu)|q\rangle &= \langle q|O^g(a)|q\rangle \Big|_{p^2=\mu^2}^{tree} = 0 \\ \langle g,\sigma|\widehat{O}^g(\mu)|g,\sigma\rangle &= \langle g,\sigma|O^g(a)|g,\sigma\rangle \Big|_{p^2=\mu^2}^{tree}.\end{aligned}\tag{44}$$

In the perturbative computation of the two members of eqs. (44) we have in our hands the choice of the polarization index σ of the external gluon (from which the Z 's obviously do not depend). To simplify our successive calculations we decided to take $\sigma \neq \mu, \nu$.

In the tree approximation the amputated non vanishing matrix elements of the operators $O_{\mu\nu}^q$ and $O_{\mu\nu}^g$ are given (for $\mu \neq \nu$, $\mu \neq \sigma$, $\nu \neq \sigma$) by

$$\begin{aligned}\langle q|O_{\mu\nu}^q(a)|q\rangle \Big|_{amp}^{tree} &= \frac{1}{2} \left[\frac{i}{2} \gamma_\mu p_\nu + (\mu \rightarrow \nu) \right] \\ \langle g,\sigma|O_{\mu\nu}^g(a)|g,\sigma\rangle \Big|_{amp}^{tree} &= -p_\mu p_\nu.\end{aligned}\tag{45}$$

From eqs. (43) and (44) the renormalization constants and the mixing coefficients of the rank two operators can be written for $\mu a \ll 1$ in the form [23, 24]

$$\begin{aligned}Z_{qq}(\mu a) &= 1 - \frac{\alpha_S}{4\pi} C_F \left(\frac{16}{3} \log \mu a + B_{qq} \right) \\ Z_{qg}(\mu a) &= -\frac{\alpha_S}{4\pi} N_f \left(\frac{4}{3} \log \mu a + B_{qg} \right) \\ Z_{gq}(\mu a) &= -\frac{\alpha_S}{4\pi} C_F \left(\frac{16}{3} \log \mu a + B_{gq} \right) \\ Z_{gg}(\mu a) &= 1 - \frac{\alpha_S}{4\pi} \left[N_f \left(\frac{4}{3} \log \mu a + B_{gg}^f \right) + N_c B_{gg} \right],\end{aligned}\tag{46}$$

where C_F and α_S have been defined in eqs. (19).

The coefficients of the logarithms are the so called anomalous dimensions. They are physical quantities and obviously their values are not affected by the improvement procedure. The difference between the use of improved and non-improved action lies only in the finite constants B . Our results for the B 's are reported in Sect. 8.

If we want operators with well defined anomalous dimensions, i.e. operators that are multiplicatively renormalizable, we must diagonalize the matrix (10) of anomalous dimensions. Its determinant, as it can be seen from (46), is zero. The two eigenvalues are

$$\begin{aligned}\gamma_1 &= 0 \\ \gamma_2 &= \frac{16}{3}C_F + \frac{4}{3}N_f,\end{aligned}\tag{47}$$

and the corresponding eigenvectors

$$\hat{O}_{\mu\nu}^1 = \left[1 - \frac{\alpha_S}{4\pi}(N_c B_{gg} + N_f(B_{gg}^f - B_{qq}))\right] O_{\mu\nu}^g - \left[1 + \frac{\alpha_S}{4\pi}C_F(B_{gq} - B_{qq})\right] O_{\mu\nu}^q\tag{48}$$

and

$$\begin{aligned}\hat{O}_{\mu\nu}^2 &= \left[1 - \frac{\alpha_S}{4\pi}(\gamma_2 \log \mu a + C_F B_{qq} + \frac{1}{4}N_f B_{gq})\right] O_{\mu\nu}^q \\ &+ \frac{N_f}{4C_F} \left[1 - \frac{\alpha_S}{4\pi}(\gamma_2 \log \mu a + 4C_F B_{gq} + N_c B_{gg} + N_f B_{gg}^f)\right] O_{\mu\nu}^g.\end{aligned}\tag{49}$$

The vanishing of one eigenvalue (γ_1) of the anomalous dimension matrix means that there exists a conserved operator (\hat{O}^1). Physically \hat{O}^1 corresponds to the full energy-momentum tensor of the system. Notice also that in the quenched approximation ($N_f = 0$) the operator \hat{O}^2 is simply proportional to O^q , as no mixing is possible with O^g in absence of quark loops.

6 Details of the computation

The improvement prescription discussed in Sect. 3 requires that in the fermion operators the spinor fields have to be rotated according to eqs. (35). This means that the improved operators are much more complicated than the non-improved ones. For instance the rank two quark operator explicitly becomes

$$\begin{aligned}
 (O_{\mu\nu}^q)^{IMPR} &= \frac{1}{4} \left[\bar{\psi} \gamma_\mu \vec{D}_\nu \psi - (\bar{\psi} \overleftarrow{D}_\nu) \gamma_\mu \psi \right] \\
 &- \frac{ar}{8} \left[\bar{\psi} \gamma_\mu \vec{D}_\nu \overrightarrow{\not{D}} \psi - (\bar{\psi} \overleftarrow{\not{D}}) \gamma_\mu \vec{D}_\nu \psi - (\bar{\psi} \overleftarrow{D}_\nu) \gamma_\mu \overrightarrow{\not{D}} \psi + (\bar{\psi} \overleftarrow{\not{D}} \overleftarrow{D}_\nu) \gamma_\mu \psi \right] \\
 &- \frac{a^2 r^2}{16} \left[(\bar{\psi} \overleftarrow{\not{D}}) \gamma_\mu \vec{D}_\nu \overrightarrow{\not{D}} \psi - (\bar{\psi} \overleftarrow{\not{D}} \overleftarrow{D}_\nu) \gamma_\mu \overrightarrow{\not{D}} \psi \right]. \tag{50}
 \end{aligned}$$

It should be noted that, although we are dealing with order a improvement, in calculating the Z 's of eqs. (43) we have to take into account also the contributions formally of order a^2 that arise when the rotations on ψ e $\bar{\psi}$ are both performed at the same time [40]. These terms in fact do contribute to the constants B because $1/a^2$ divergences present in 1-loop lattice diagrams can compensate the factor a^2 in front of them, thus giving rise to finite contributions to the Z 's. Since in actual Monte Carlo simulations each ψ or $\bar{\psi}$ field is subjected to the whole rotation (35) [19], the full expression (50) must be considered in the calculation of renormalization constants and mixing coefficients.

In the presentation of the computations in Sect. 8 we have for convenience separated all these various contributions. We will thus consider in turn diagrams with the insertion of the non-rotated (non-improved) operator, diagrams with the insertion of only one rotation, either on ψ or on $\bar{\psi}$, and diagrams with the insertion of both rotations. The operator (50) has been expanded in powers of g_0 up to order g_0^2 . This is sufficient for our 1-loop calculations. The corresponding formulae have been computed by hand and

then checked by means of the algebraic manipulation language Schoonschip, and are summarized in appendix A.

Consequently to the use of improvement, there is a very large number of diagrams to be computed (see appendix B) and, a part from few cases, the algebraic manipulations of every diagram give rise to a huge number of terms. For this reason it has been necessary to check independently all the computations by using Schoonschip. We have to this end developed a general program that is able to automatically carry out all the algebraic manipulations starting from the elementary building blocks of the calculation, represented by the expressions of propagators and vertices. The final output of the program is an analytic expression of the Z 's under the form of a 1-loop integral.

A large part of this work has thus been spent in developing an efficient Schoonschip code adapted to the problem at hand. The main difficulty resides in the fact that, although there are many built in instructions to deal with gamma matrices, Schoonschip has been conceived having in mind a continuum theory, which is invariant with respect to the (euclidean) Lorentz group. On the lattice, on the contrary, the theory is only invariant with respect to the hypercubic group, and unfortunately many simple and common terms like $\sum_{\lambda} \gamma_{\lambda} p_{\lambda} \sin k_{\lambda}$ that arise on the lattice are not properly handled. Actually, the above term is wrongly reduced by Schoonschip to $\not{p} \sin k_{\lambda}$, because two equal indices are by default assumed to be contracted. Furthermore the result depends on the order in which the various factors are encountered, because the Lorentz invariant summation is immediately performed between the first two indexed quantities encountered in the analytic expression.

Being impossible to directly use the “gammatric” of Schoonschip as it is, a special routine has been developed to correctly treat gamma matrices on the lattice while using as much as possible of the built in Schoonschip

commands².

As we said, for each contribution the program starts with the expression of the corresponding Feynman diagram in terms of propagators and vertices. Before carrying out the Dirac algebra, one can simplify the expressions by noticing that in the final loop integration one will have to integrate products of sines with functions of cosines and of H(4) invariant combinations of sines. Odd products of sines integrate to zero, while even products will lead to integrals of the type

$$\mathcal{I}(\mu_1, \dots, \mu_{2n}) = \int d^4k f(\cos k, \sum_{\lambda} \sin^2 k_{\lambda}) \prod_{i=1}^{2n} \sin k_{\mu_i}, \quad (51)$$

where f is an H(4) covariant function. Exploiting the symmetry of the integration measure under H(4), the integrand (51) can be expressed in terms of a certain number of simpler integrals. For instance for $n = 2$ one has

$$\begin{aligned} \mathcal{I}(\mu_1, \mu_2, \mu_3, \mu_4) &= \int d^4k f(\cos k, \sum_{\lambda} \sin^2 k_{\lambda}) \sin k_{\mu_1} \sin k_{\mu_2} \sin k_{\mu_3} \sin k_{\mu_4} = \\ &\int d^4k f(\cos k, \sum_{\lambda} \sin^2 k_{\lambda}) \sin^2 k_{\mu_1} \sin^2 k_{\mu_3} \delta_{\mu_1\mu_2} \delta_{\mu_3\mu_4} \\ &+ \int d^4k f(\cos k, \sum_{\lambda} \sin^2 k_{\lambda}) \sin^2 k_{\mu_1} \sin^2 k_{\mu_2} \delta_{\mu_1\mu_3} \delta_{\mu_2\mu_4} \\ &+ \int d^4k f(\cos k, \sum_{\lambda} \sin^2 k_{\lambda}) \sin^2 k_{\mu_1} \sin^2 k_{\mu_2} \delta_{\mu_1\mu_4} \delta_{\mu_2\mu_3} \\ &- 2 \cdot \int d^4k f(\cos k, \sum_{\lambda} \sin^2 k_{\lambda}) \sin^4 k_{\mu_1} \delta_{\mu_1\mu_2\mu_3\mu_4}, \end{aligned} \quad (52)$$

where $\delta_{\mu_1\mu_2\mu_3\mu_4}$ is non-zero only if all the indices are equal.

The case $n = 1$ is trivial. A 6-sine term ($n = 3$) instead gives rise to a combination of 31 terms. In the calculation of $\langle q|(O_{\mu\nu\tau}^q)^{IMPR}|q \rangle$ [11] one also encounters some 8-sine terms ($n = 4$), each one giving rise to 379

²We are willing to send our codes to anyone interested.

terms. A brief discussion of these expansions and of their derivation is given in appendix C.

The rather complicated Dirac algebra (we have products of up to 7 gamma matrices) is carried out at this point, exploiting the δ -functions that are expected to come out from the loop integration, as exemplified in eq. (52). The last step consists in extracting the Z factors by projecting the whole expression on the appropriate tensor structure (see eqs. (45)).

The CPU time needed to perform the whole analytic calculation varies according to the complexity of the diagram, going from 20 seconds up to 5 minutes for the most complicated cases on a Sun 3 workstation.

7 Loop integration

The resulting analytic expressions must be finally integrated in momentum space over the first Brillouin zone. We want to compute all these integrals with a total error of about 1%, in order not to spoil the accuracy aimed at with the use of improvement.

In almost all diagrams there will be an extra integration over a Feynman parameter α . Since it turned out to be exceedingly time consuming to evaluate our five dimensional integrals with an error of less than 1%, we decided to perform analytically the α integration, writing the result in terms of the functions

$$F_{nm}(f(k), g(k)) = \int_0^1 d\alpha \frac{\alpha^n}{[f(k) + \alpha g(k)]^m}. \quad (53)$$

These functions, for the values of n and m relevant for this work, are tabulated in appendix D. The remaining four dimensional integrals are afterwards numerically computed with the most naive rectangular method, i.e. by summing over a uniformly distributed net of points.

All integrals are at most logarithmically divergent in the limit $a\mu \rightarrow 0$

and have been computed by adding and subtracting to them known integrals with integrand functions having identical leading “ $1/k^2$ ” and “ $1/k^4$ ” lattice behavior, as the original integrands. The final step consists in evaluating numerically the resulting finite integrals. In this way one can easily obtain the required precision with reasonable computing times.

As for the “ $1/k^2$ ” part, one subtracts and adds with the appropriate coefficients the integral

$$\int_{-\pi}^{\pi} \frac{d^4k}{(2\pi)^4} \cdot \frac{1}{[4 \sum_{\lambda} \sin^2 \frac{k_{\lambda}}{2}]} = Z_0, \quad (54)$$

whose value can be found in Table 7.1.

Z_0	0.15493339
Z_1	0.10778131
F_0	4.36922523
γ_E	0.57721566

Table 7.1 - Values of some useful lattice constants

For the logarithmically divergent part we actually use a double subtraction. To explain the method, let us consider a typical integral of the form

$$I = \int_0^1 d\alpha \int_{-\pi}^{\pi} \frac{d^4k}{(2\pi)^4} \frac{N(k)}{[D(k; \alpha) + \alpha(1 - \alpha)\mu^2 a^2]^2}, \quad N(0) \neq 0, \quad (55)$$

where

$$D(k; \alpha) = 4\alpha \sum_{\lambda} \sin^2 \frac{k_{\lambda}}{2} + (1 - \alpha) [\sum_{\lambda} \sin^2 k_{\lambda} + 4r^2 (\sum_{\lambda} \sin^2 \frac{k_{\lambda}}{2})^2] \quad (56)$$

and, for instance,

$$N(k) = \cos k_{\mu}. \quad (57)$$

I could be computed by summing and subtracting to it the known integral

$$\begin{aligned}
I_0 &= \int_0^1 d\alpha \int_{-\pi}^{\pi} \frac{d^4 k}{(2\pi)^4} \frac{N(0)}{[4 \sum_{\lambda} \sin^2 \frac{k_{\lambda}}{2} + \alpha(1-\alpha)\mu^2 a^2]^2} \\
&= \frac{N(0)}{16\pi^2} \cdot \left[-\log \mu^2 a^2 - \int_0^1 d\alpha \log \alpha(1-\alpha) - \gamma_E + F_0 \right] + O(a\mu), \quad (58)
\end{aligned}$$

where F_0 is given in Table 7.1 together with the Euler-Mascheroni constant γ_E . In this way one can write

$$I = (I - I_0) + \frac{N(0)}{16\pi^2} \cdot \left[-\log \mu^2 a^2 + 2 - \gamma_E + F_0 \right] + O(a\mu). \quad (59)$$

$I - I_0$ is finite as $a\mu \rightarrow 0$ and can be safely evaluated in this limit. However, the denominators in (55) and (58) are different, and this can lead to numerical errors larger than 1%, if one does not use a sufficiently large number of points, because the matching of divergent parts may not be sufficiently good in correspondence to the smallest value of k in the mesh of points one has taken.

The results presented in literature for this kind of integrals generally use Monte Carlo integrations. With this method one can hardly explore the low k region with an adequate number of samplings, therefore there is a (small (?)) finite rest overlooked by the numerical integration. To overcome this problem (which is also present, though to a lesser extent, in the rectangle integration) and to reduce the number of different integrals to be computed numerically, we have employed a more refined subtraction procedure.

The idea is to perform a double subtraction in order to match separately the form of the numerators and of the denominators appearing in the various integrals. To do this, we introduce the auxiliary quantity

$$I_1 = \int_0^1 d\alpha \int_{-\pi}^{\pi} \frac{d^4 k}{(2\pi)^4} \frac{N(0)}{[D(k; \alpha)]^2} \quad (60)$$

and we write

$$I = I_0 + (I_1 - I_0) + (I - I_1). \quad (61)$$

Of course both differences, $I_1 - I_0$ and $I - I_1$, are finite as $a\mu \rightarrow 0$ and can be computed directly at $a\mu = 0$. Explicitly one gets

$$\lim_{a\mu \rightarrow 0} (I - I_1) = \int_0^1 d\alpha \int_{-\pi}^{\pi} \frac{d^4 k}{(2\pi)^4} \frac{N(k) - N(0)}{[D(k; \alpha)]^2} \quad (62)$$

and

$$\begin{aligned} \lim_{a\mu \rightarrow 0} (I_1 - I_0) &= N(0) \cdot \int_0^1 d\alpha \int_{-\pi}^{\pi} \frac{d^4 k}{(2\pi)^4} \left[\frac{1}{[D(k; \alpha)]^2} - \frac{1}{[4 \sum_{\lambda} \sin^2 \frac{k_{\lambda}}{2}]^2} \right] \\ &= N(0) \cdot \int_0^1 d\alpha \int_{-\pi}^{\pi} \frac{d^4 k}{(2\pi)^4} \cdot \\ &\cdot \left[\frac{[4 \sum_{\lambda} \sin^2 \frac{k_{\lambda}}{2}]^2 - [4\alpha \sum_{\lambda} \sin^2 \frac{k_{\lambda}}{2} + (1 - \alpha)[\sum_{\lambda} \sin^2 k_{\lambda} + 4r^2(\sum_{\lambda} \sin^2 \frac{k_{\lambda}}{2})^2]]^2}{[4\alpha \sum_{\lambda} \sin^2 \frac{k_{\lambda}}{2} + (1 - \alpha)[\sum_{\lambda} \sin^2 k_{\lambda} + 4r^2(\sum_{\lambda} \sin^2 \frac{k_{\lambda}}{2})^2]]^2 [4 \sum_{\lambda} \sin^2 \frac{k_{\lambda}}{2}]^2} \right]. \end{aligned} \quad (63)$$

We see that in eq. (62) the two integrands have the same denominator, while in eq. (63) the two integrands have the same numerator. The cancellation of the logarithmic divergences, between the two terms of eq. (63), has been made explicit in the last equality by the exact compensation of the leading $1/k^4$ behaviors of the two integrands.

The double subtraction method we have explained reduces to only five the number of different types of integrals that are in the end necessary to express all the differences, similar to those appearing in eq. (61), that arise in the diagrams one needs to compute.

In the case of diagrams which contain only gluons, we have used the method suggested by Caracciolo, Menotti e Pelissetto [17] which allows to iteratively reduce all integrals to few basic integrals which are known with great precision.

8 Results

The results of our calculations are summarized in the Tables 8.1 to 8.6 presented in this section. The contributions coming from the standard Wilson action (that is, the non-improved results), those coming from the terms of order a in the improvement and those coming from the terms of order a^2 are separately shown. Contributions coming from different classes of diagrams, according to the classification given in appendix B, are also separately presented. In Tables 8.7 and 8.8 we detail the comparison of our results with those of ref. [17].

In the quenched approximation ($N_f = 0$) B_{gg} and B_{gg}^f disappear from eqs. (48) and (49), and even in the flavor singlet sector the quark operator does not mix with the gluon operator, as the matrix (38) becomes triangular. In the full theory ($N_f \neq 0$, “unquenched”) we have on the contrary complete mixing between the quark operator, O^q , and the gluon operator, O^g . To compute in this case the renormalization constants and mixing coefficients we need also to evaluate the diagrams of Figs. 6 and 7 of appendix B, corresponding to respectively the matrix element $\langle g, \sigma | (O_{\mu\nu}^q)^{IMPR} | g, \sigma \rangle$ and the quark loop contribution to the matrix element $\langle g, \sigma | O_{\mu\nu}^g | g, \sigma \rangle$.

In Table 8.5 one can find the analytic expression of B_{gg} leading, through the use of Table 7.1, to the numerical values shown in Table 8.4.

The contributions to $\langle g, \sigma | O_{\mu\nu}^g | g, \sigma \rangle$ of the diagrams labeled as “tadpole-QCD vertex” and “tadpole-quark loop” in appendix B are zero, and have not been inserted in Tables 8.4 and 8.5.

As emphasized in the previous section, the accuracy of our results is better than 1%. The differences we have found by comparing our results for the Wilson case with results previously appeared in the literature [12, 13, 14, 15] come from either insufficient accuracy in the Monte Carlo numerical integration or trivial algebraic mistakes. However, we are in complete agreement

	r	Wilson	$O(a)$ impr.	$O(a^2)$ impr.	total
SAILS	0.2	-1.970	-1.746	-0.026	-3.742
	0.4	-3.081	-4.014	-0.173	-7.267
	0.6	-3.935	-5.524	-0.487	-9.946
	0.8	-4.576	-6.458	-0.972	-12.007
	1.0	-5.077	-7.041	-1.626	-13.744
VERTEX	0.2	0.555	-0.132	0.017	0.440
	0.4	1.038	-0.470	0.109	0.678
	0.6	1.535	-0.821	0.290	1.004
	0.8	1.952	-1.128	0.555	1.379
	1.0	2.293	-1.389	0.904	1.808
$\frac{1}{2}$ SELF-ENERGY	0.2	-6.102	-0.611	0	-6.713
	0.4	-4.326	-1.513	0	-5.839
	0.6	-2.762	-2.311	0	-5.073
	0.8	-1.465	-3.013	0	-4.479
	1.0	-0.381	-3.646	0	-4.027
operator TADPOLE + $\frac{1}{2}$ leg TADPOLE	0.2	0	0	0.006	0.006
	0.4	0	0	0.024	0.024
	0.6	0	0	0.053	0.053
	0.8	0	0	0.095	0.095
	1.0	0	0	0.148	0.148
TOTAL	0.2	-7.517	-2.489	-0.003	-10.010
	0.4	-6.369	-5.996	-0.040	-12.404
	0.6	-5.161	-8.657	-0.143	-13.961
	0.8	-4.090	-10.600	-0.322	-15.012
	1.0	-3.165	-12.076	-0.575	-15.816

Table 8.1 - Values of B_{qq}

r	Wilson	$O(a)$ impr.	$O(a^2)$ impr.	total
0.2	-5.184	-0.029	-0.010	-5.223
0.4	-1.609	-0.298	-0.038	-1.945
0.6	-0.704	-0.582	-0.063	-1.349
0.8	-0.276	-0.782	-0.100	-1.158
1.0	0.019	-0.906	-0.154	-1.041

Table 8.2 - Values of B_{gg}

r	Wilson	$O(a)$ impr.	total
0.2	-3.722	0.217	-3.505
0.4	-4.372	0.628	-3.744
0.6	-4.938	1.044	-3.894
0.8	-5.413	1.427	-3.986
1.0	-5.817	1.773	-4.044

Table 8.3 - Values of B_{gq}

	Wilson
SAILS	-4.453
VERTEX	5.019
operator TADPOLE	$-40.024 + 4\pi^2/N_c^2$
$\frac{1}{2}$ leg TADPOLE	$19.207 - 2\pi^2/N_c^2$
$\frac{1}{2}$ gluon LOOP	2.274
$\frac{1}{2}$ GHOST	0.198
TOTAL	$-17.778 + 2\pi^2/N_c^2$

Table 8.4 - Values of B_{gg}

SAILS	$\frac{1}{192} - \frac{7}{9\pi^2} + \frac{31}{24}Z_0 - \frac{19}{48}Z_1 - \frac{7}{24\pi^2} \cdot (F_0 - \gamma_E)$
VERTEX	$-\frac{13}{192} + \frac{23}{48\pi^2} - \frac{53}{144}Z_0 + \frac{1}{3}Z_1 + \frac{3}{16\pi^2} \cdot (F_0 - \gamma_E)$
operator TADPOLE	$-\frac{3}{64} - \frac{4}{3}Z_0 + \frac{1}{4N_c^2}$
$\frac{1}{2}$ leg TADPOLE	$\frac{1}{32} + \frac{7}{12}Z_0 - \frac{1}{8N_c^2}$
$\frac{1}{2}$ gluon LOOP	$\frac{1}{32} + \frac{13}{72\pi^2} - \frac{17}{36}Z_0 + \frac{19}{192\pi^2} \cdot (F_0 - \gamma_E)$
$\frac{1}{2}$ GHOST	$\frac{1}{72\pi^2} - \frac{1}{72}Z_0 + \frac{1}{192\pi^2} \cdot (F_0 - \gamma_E)$
TOTAL	$-\frac{3}{64} - \frac{5}{48\pi^2} - \frac{5}{16}Z_0 - \frac{1}{16}Z_1 + \frac{1}{8N_c^2}$

Table 8.5 - Analytic expressions of $B_{gg}/(16\pi^2)$. The constants Z_0 , Z_1 , F_0 and γ_E can be found in Table 7.1. Each line in this Table equals the sum of the corresponding two in Tables 8.7 and 8.8.

	r	Wilson	$O(a)$ impr.	total
$\frac{1}{2}$ quark LOOP	0.2	-13.473	-27.475	-40.948
	0.4	-5.643	-32.141	-37.784
	0.6	-3.512	-27.057	-30.570
	0.8	-2.656	-21.581	-24.237
	1.0	-2.168	-17.257	-19.425

Table 8.6 - Values of B_{gg}^f

with the results for the energy-momentum tensor given in refs. [16] and [17], as well as with the gluon self-energy reported in [41].

To check the value of Z_{qq} , it is enough to take the corresponding quantity, called Z_1 in Table 1 of ref. [16], and multiply it by -8 and $16\pi^2$ to find

$$B_{qq} \text{ (from ref. [16])} = -8 \cdot 16\pi^2 \cdot (0.00252), \quad (64)$$

in agreement (within numerical accuracy) with the number given in the last line of Table 8.1:

$$B_{qq} = -3.165. \quad (65)$$

To compare the results for Z_{gg} with those of ref. [17] one must take into account that two different regularization procedures have been employed to deal with logarithmically divergent loop integrals. We have regularized all integrals by putting the external legs infinitesimally off-shell by an amount $\mu^2 \ll 1/a^2$, while in ref. [17] each term, I , is expanded up to second order in the four-vector of the external legs, p , and decomposed in $H(4)$ tensors. Dimensional regularization is used to compute loop integrals. Calling J , as in ref. [17], the relevant terms of this expansion, it is easy to see that the

difference $I - J$ (for small p) can in fact be computed as a continuum integral³, since its value only depends on the behavior of the integrand at $k = 0$.

To explicitly carry on the comparison with ref. [17] we have thus computed using dimensional regularization $I - J$ for small p . We report their values in Table 8.7, apart from the logarithmic terms we always have singled out in all formulae. We collect in Table 8.8 the values of J , obtained from ref. [17] remembering that in the Tables presented there our operator (13) corresponds in their notations to the tensor structure $L_3 - L_{10}$. As announced, the sum $J + (I - J)$ reproduce exactly the results given in our Table 8.5.

Obviously physical quantities will be at the end independent from the chosen regularization procedure. In particular the dependence from the subtraction point, μ , must disappear from physical hadronic matrix elements. In fact, consistently to each order in perturbation theory, the $\log \mu$ terms get canceled in the product between the Wilson coefficients and the matrix elements of the renormalized operators that are eigenvectors of the anomalous dimension matrix. The net result is that effectively the Wilson coefficients must be taken at a momentum scale a^{-1} and the operators (48) and (49) renormalized by reduced renormalization constants, obtained from the full expressions by dropping all logarithmic terms.

The effective renormalization of the bare quark operator is rather small. Numerically for $N_c = 3$ at the typical values $\beta \equiv 2N_c/g_0^2 = 6$ and $r = 1$, one gets in the quenched approximation for the unmixed quark operator

$$\begin{aligned} \tilde{O}_{\mu\nu}^2 &= 1.027 O_{\mu\nu}^q && \text{Wilson case} \\ (\tilde{O}_{\mu\nu}^2)^{IMPR} &= 1.134 (O_{\mu\nu}^q)^{IMPR} && \text{Improved case ,} \end{aligned}$$

where by the superscript \sim we mean that the $\log \mu$ term contribution has been dropped from the expression of the Z 's with the understanding that the corresponding Wilson coefficients are computed at a scale $\mu = 1/a$.

³This is why only the genuinely lattice dependent quantity J is reported in ref. [17].

SAILS	$-\frac{7}{24\pi^2} \cdot \left(\frac{2}{\varepsilon} + \log 4\pi - \gamma_E\right)$
VERTEX	$\frac{7}{24\pi^2} + \frac{3}{16\pi^2} \cdot \left(\frac{2}{\varepsilon} + \log 4\pi - \gamma_E\right)$
operator TADPOLE	0
$\frac{1}{2}$ leg TADPOLE	0
$\frac{1}{2}$ gluon LOOP	$\frac{29}{144\pi^2} + \frac{19}{192\pi^2} \cdot \left(\frac{2}{\varepsilon} + \log 4\pi - \gamma_E\right)$
$\frac{1}{2}$ GHOST	$\frac{1}{72\pi^2} + \frac{1}{192\pi^2} \cdot \left(\frac{2}{\varepsilon} + \log 4\pi - \gamma_E\right)$
TOTAL $I - J$	$\frac{73}{144\pi^2}$

Table 8.7 - The contribution to the analytic expression of $B_{gg}/(16\pi^2)$, called $I - J$ in the text, according to the definition given in ref. [17].

SAILS	$\frac{1}{192} - \frac{7}{9\pi^2} + \frac{31}{24}Z_0 - \frac{19}{48}Z_1 - \frac{7}{24\pi^2} \cdot \left(-\frac{2}{\varepsilon} + F_0 - \log 4\pi \right)$
VERTEX	$-\frac{13}{192} + \frac{3}{16\pi^2} - \frac{53}{144}Z_0 + \frac{1}{3}Z_1 + \frac{3}{16\pi^2} \cdot \left(-\frac{2}{\varepsilon} + F_0 - \log 4\pi \right)$
operator TADPOLE	$-\frac{3}{64} - \frac{4}{3}Z_0 + \frac{1}{4N_c^2}$
$\frac{1}{2}$ leg TADPOLE	$\frac{1}{32} + \frac{7}{12}Z_0 - \frac{1}{8N_c^2}$
$\frac{1}{2}$ gluon LOOP	$\frac{1}{32} - \frac{1}{48\pi^2} - \frac{17}{36}Z_0 + \frac{19}{192\pi^2} \cdot \left(-\frac{2}{\varepsilon} + F_0 - \log 4\pi \right)$
$\frac{1}{2}$ GHOST	$-\frac{1}{72}Z_0 + \frac{1}{192\pi^2} \cdot \left(-\frac{2}{\varepsilon} + F_0 - \log 4\pi \right)$
TOTAL J	$-\frac{3}{64} - \frac{11}{18\pi^2} - \frac{5}{16}Z_0 - \frac{1}{16}Z_1 + \frac{1}{8N_c^2}$

Table 8.8 - The contribution to the analytic expression of $B_{gg}/(16\pi^2)$, called J in the text, according to the definition given in ref. [17].

The gluonic contribution to the energy-momentum tensor operator, whose hadronic matrix elements are incidentally very difficult to measure in Monte Carlo simulations [13], are somewhat larger. One gets in fact for \widehat{O}^1

$$\begin{aligned} \widehat{O}_{\mu\nu}^1 &= 1.296 O_{\mu\nu}^g - 0.978 O_{\mu\nu}^q && \text{Wilson case} \\ (\widehat{O}_{\mu\nu}^1)^{IMPR} &= 1.296 O_{\mu\nu}^g - 1.099 (O_{\mu\nu}^q)^{IMPR} && \text{Improved case .} \end{aligned}$$

There are suggestions that the large renormalizations in the gluon sector come from the choice of the bare lattice coupling as expansion parameter [42]. Actually, a very large renormalization factor relates the bare lattice coupling to the continuum one (as calculated for example in the \overline{MS} scheme [43]). It is also believed that the large contributions coming from tadpole diagrams are the main source of numerical discrepancies between continuum and lattice perturbation theory.

According to ref. [44], a resummation of tadpole contributions could be effectively achieved if the perturbative series is expanded in terms of a “boosted” coupling constant

$$\tilde{g} = \frac{g_0}{u_0^2}, \quad (66)$$

where $u_0 (< 1)$ should be taken as the non-perturbative mean value of the link operator. A convenient measure of u_0 can be obtained from the plaquette expectation value (eq. 31)

$$u_0 = \left\langle \frac{1}{3} \text{Tr} U_{n,\mu\nu} \right\rangle^{1/4}. \quad (67)$$

Here a first question arises whether or not tadpole diagrams should be re-traced from perturbative results, as they are effectively already taken into account in the redefinition (66).

Another problem is that u_0 could also be measured from the renormalization of the Wilson hopping parameter, by writing

$$K_c = \frac{1}{8 \cdot u_0}. \quad (68)$$

The definition (68), contrary to the one given by eq. (67), depends upon the choice of the fermion part of the QCD action⁴. It should be observed here that, when using eq. (68), one should for consistency perhaps also introduce an explicit correction for the large deviation between the perturbative and the non-perturbative quark mass renormalization⁵, besides changing the value of the effective expansion parameter.

Because of the many subtleties involved in the whole question of “boosting” perturbation theory, we like to refrain from attempting any numerical evaluation of the effects of these corrections to our numbers, and we rather like to present the results of our calculations as they appears in terms of the bare coupling constant, leaving any other numerical consideration to actual applications.

9 Conclusions and outlook

As we have briefly discussed in Sect. 3, a simple modification of the fermion action, accompanied by a suitable redefinition of hadronic operators, leads to the theoretical expectation of an “effective $O(a)$ ” improvement in on-shell hadronic matrix elements [8]. This was indeed beautifully confirmed by the exploratory numerical Monte Carlo simulations of refs. [19] and [20].

After these encouraging results there has been a general agreement that the new high-statistics QCD Monte Carlo simulations that are planned to use next generation dedicated machines (e.g. APE with ≥ 6 Gflops) should all be performed with the “clover-leaf” improved action.

This paper and the forthcoming one, that are dealing with respectively

⁴It is interesting to note that, unlike the Wilson case, the two definitions (67) and (68) seem to lead to numerically very close values in the case of the “clover-leaf” action [45].

⁵We wish to thank G.Martinelli for a discussion about this point.

the first and the second moment of DIS structure functions, are part of the general project aimed at the perturbative recalculation with the “clover-leaf” improved action of all the renormalization constants and mixing coefficients of the fermion operators whose matrix elements are phenomenologically relevant and susceptible of being measured in Monte Carlo simulations.

To complete the analytic part of the above program only the mixing coefficient between the dimension six four-fermion $\Delta I = 1/2$ effective weak Hamiltonian and the dimension five operator appearing in eq. (30) is missing. In the standard Wilson theory this finite (thanks to the GIM mechanism) coefficient was computed in ref. [46]. Its calculation in the case of the “clover-leaf” improved action is presently under way [47].

We think it is fair to conclude this paper with a remark on the reliability of lattice perturbation theory itself, which looks even more problematic than continuum perturbation theory. For instance, gluonic corrections tend to be anomalously big because of large tadpole contributions. As we remarked in Sect. 8, one possible remedy could be to use a better expansion parameter than the bare coupling constant, as advocated in refs. [42] and [44], in a way to effectively incorporate a resummation of these large tadpole diagrams.

A perhaps more promising and consistent way to proceed has been, however, recently suggested in ref. [48]. The idea is to extract renormalization constants directly from Monte Carlo data, by measuring matrix elements of hadronic operators between quark states and exploiting information coming from Ward identities. Such a procedure would eliminate altogether lattice perturbation theory from the game. This fact might be regarded as rather satisfactory for a numerical approach like the lattice one which, taken in its most extreme formulation, should refrain from using any kind of (approximate or unreliable) perturbative calculations.

Acknowledgments

We would like to thank Sergio Caracciolo, Pietro Menotti and Andrea Pelissetto for their patience in helping us to compare their calculations with ours. We also thank Giuseppe Beccarini for checking some of our Schoonschip outputs. S.C. would like to thank Guido Martinelli and Massimo Testa for introducing him to lattice QCD, Enrico Franco, Roberto Frezzotti, Emidio Gabrielli and Carlotta Pittori for help at the initial stage of this work and Ugo Aglietti for useful hints about numerical integration.

Appendix A

Perturbative expansion of the vertex operators

$(O_{\mu\nu}^q)^{IMPR}$ and $O_{\mu\nu}^g$

In this appendix we give the perturbative expansion of the vertex operators $(O_{\mu\nu}^q)^{IMPR}$, given by eq. (50), and $O_{\mu\nu}^g$, given by eq. (13) with the insertion of the definition (32). We used the covariant derivatives defined as

$$\vec{D}_\mu \psi_n = \frac{1}{2a} [U_{n,\nu} \psi_{n+\mu} - U_{n-\mu,\mu}^+ \psi_{n-\mu}] \quad (69)$$

$$\overline{\psi} \overleftarrow{D}_\mu = \frac{1}{2a} [\overline{\psi}_{n+\mu} U_{n,\nu}^+ - \overline{\psi}_{n-\mu} U_{n-\mu,\mu}],$$

and the conventions

$$A_{n,\mu} = \int \frac{d^4 q}{(2\pi)^4} e^{i(q + q_\mu/2)n} A_\mu(q) \quad (70)$$

$$\psi_n = \int \frac{d^4 q}{(2\pi)^4} e^{iqn} \psi(q) \quad (71)$$

$$\overline{\psi}_n = \int \frac{d^4 q}{(2\pi)^4} e^{-iqn} \overline{\psi}(q), \quad (72)$$

where the integrals are performed over the first Brillouin zone. Throughout this appendix external and loop momenta are expressed in lattice units.

Since the full Fourier transform of the operator $(O_{\mu\nu}^q)^{IMPR}$ is very complicated, we give here only the form it effectively takes when inserted in the diagrams of Figs. 2, 3, 4 and 7. Calling p the external incoming and outgoing momentum, and k the fermion loop momentum, one finds, separating the various contributions according to their naive order in a :

a) tree level

$$(O_{\mu\nu}^q)^{IMPR}(n=0)|_{tree} = \frac{i}{2} \int_{-\pi}^{\pi} \frac{d^4 k}{(2\pi)^4} \overline{\psi}(k) \gamma_\mu \frac{\sin k_\nu}{a} \psi(k)$$

$$\begin{aligned}
& + \frac{ar}{2} \int_{-\pi}^{\pi} \frac{d^4k}{(2\pi)^4} \bar{\psi}(k) \frac{\sin k_\mu \sin k_\nu}{a} \psi(k) \\
& - \frac{ia^2r^2}{8} \int_{-\pi}^{\pi} \frac{d^4k}{(2\pi)^4} \bar{\psi}(k) \sum_{\lambda, \lambda'} \gamma_\lambda \gamma_\mu \gamma_{\lambda'} \frac{\sin k_\lambda \sin k_{\lambda'}}{a} \frac{\sin k_\nu}{a} \psi(k).
\end{aligned} \tag{73}$$

b) order g_0

$$\begin{aligned}
(O_{\mu\nu}^q)^{IMPR}(n=0)|_{g_0} & = \frac{ig_0}{2} \int_{-\pi}^{\pi} \frac{d^4k}{(2\pi)^4} \bar{\psi}(p) \gamma_\mu \left[\cos\left(\frac{k+p}{2}\right)_\nu A_\nu(p-k) \right] \psi(k), \\
& + \frac{ag_0r}{4} \int_{-\pi}^{\pi} \frac{d^4k}{(2\pi)^4} \bar{\psi}(p) \sum_\lambda \left[\cos\left(\frac{k+p}{2}\right)_\nu \left(\gamma_\mu \gamma_\lambda \frac{\sin k_\lambda}{a} + \gamma_\lambda \gamma_\mu \frac{\sin p_\lambda}{a} \right) A_\nu(p-k) \right. \\
& \quad \left. + \cos\left(\frac{k+p}{2}\right)_\lambda \left(\gamma_\mu \gamma_\lambda \frac{\sin p_\nu}{a} + \gamma_\lambda \gamma_\mu \frac{\sin k_\nu}{a} \right) A_\lambda(p-k) \right] \psi(k) \\
& - \frac{ia^2g_0r^2}{8} \int_{-\pi}^{\pi} \frac{d^4k}{(2\pi)^4} \bar{\psi}(p) \sum_{\lambda, \lambda'} \gamma_\lambda \gamma_\mu \gamma_{\lambda'} \left[\cos\left(\frac{k+p}{2}\right)_\nu A_\nu(p-k) \frac{\sin k_{\lambda'}}{a} \frac{\sin p_\lambda}{a} \right. \\
& \quad \left. + \cos\left(\frac{k+p}{2}\right)_\lambda A_\lambda(p-k) \frac{\sin k_{\lambda'}}{a} \frac{\sin k_\nu}{a} \right. \\
& \quad \left. + \cos\left(\frac{k+p}{2}\right)_{\lambda'} A_{\lambda'}(p-k) \frac{\sin p_\lambda \sin p_\nu}{a} \right] \psi(k).
\end{aligned} \tag{74}$$

This formula is given in the kinematical configuration in which the incoming gluon momentum lands on the incoming quark leg. If the gluon is attached to the outgoing quark leg, one must exchange p and k . Notice that the first lines in eqs. (73) and (74) correspond to the non-improved expression of the operator.

We do not give here the expression of the $O(g_0^2)$ terms because, besides being extremely complicated, they are not actually necessary for our computation. In fact we need them only when either the gluon or the quark legs are contracted to make a tadpole loop, and in this situation the tadpole directly factorizes out.

On the gluon operator $O_{\mu\nu}^g$ there is no effect due to the improvement, because the transformation (35) acts only on spinors, and one finds:

a) tree level

$$\begin{aligned}
O_{\mu\nu}^g(n=0)|_{tree} &= -\frac{1}{2} \sum_{\rho} \int \frac{dq_1 dq_2}{(2\pi)^4} \delta^{(4)}(q_1 + q_2) \\
&\frac{1}{a} \left(A_{\mu}^a(q_1) \cos \frac{q_{1\mu}}{2} \sin q_{1\rho} - A_{\rho}^a(q_1) \cos \frac{q_{1\rho}}{2} \sin q_{1\mu} \right) \\
&\cdot \frac{1}{a} \left(A_{\rho}^a(q_2) \cos \frac{q_{2\rho}}{2} \sin q_{2\nu} - A_{\nu}^a(q_2) \cos \frac{q_{2\nu}}{2} \sin q_{2\rho} \right). \tag{75}
\end{aligned}$$

b) order g_0

$$\begin{aligned}
O_{\mu\nu}^g(n=0)|_{g_0} &= -\frac{ig_0}{4} f^{abc} \sum_{\rho} \int \frac{dq_1 dq_2 dq_3}{(2\pi)^8} \delta^{(4)}(q_1 + q_2 + q_3) \\
&\frac{1}{a} \cdot \left[A_{\mu}^a(q_1) \cos \frac{q_{1\mu}}{2} \sin q_{1\rho} - A_{\rho}^a(q_1) \cos \frac{q_{1\rho}}{2} \sin q_{1\mu} \right] \\
&\cdot \left[A_{\rho}^b(q_2) A_{\nu}^c(q_3) \left[\left(\cos \frac{q_{2\rho}}{2} - \cos \frac{(q_2 + 2q_3)_{\rho}}{2} \right) \cdot \left(\cos \frac{q_{3\nu}}{2} - \cos \frac{(q_3 + 2q_2)_{\nu}}{2} \right) \right. \right. \\
&- 2 \cos \frac{(q_2 + 2q_3)_{\rho}}{2} \cos \frac{(q_3 + 2q_2)_{\nu}}{2} \left. \left. \right] - A_{\rho}^b(q_2) A_{\rho}^c(q_3) \sin \frac{(q_2 + q_3)_{\rho}}{2} \sin q_{3\nu} \right. \\
&\left. \left. + A_{\nu}^b(q_2) A_{\nu}^c(q_3) \sin \frac{(q_2 + q_3)_{\nu}}{2} \sin q_{3\rho} \right] + (\mu \rightarrow \nu). \tag{76}
\end{aligned}$$

As for the $O(g_0^2)$ terms we do not report here their expression for the same reasons explained after eq. (74).

Appendix B

Diagrams

In what follows we show all the 1-loop diagrams that have been calculated in the context of this work. Many of them have a label that allows an easy connection with the Tables presented in Sect. 8.

Actually, each graph in this appendix corresponds to several diagrams in the perturbative expansion. For example, the vertex correction of Fig. 2

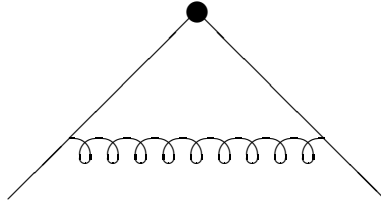
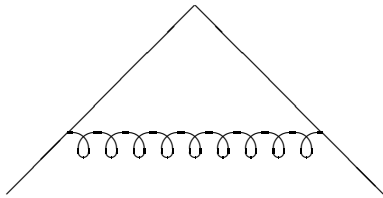
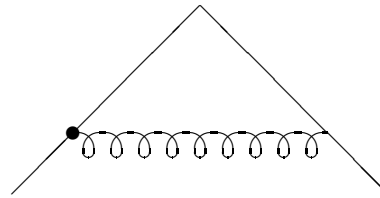


Fig. 2 - The graph that symbolically represents the 1-loop correction to the insertion of the $(O_{\mu\nu}^q)^{IMPR}$ operator. The insertion is indicated by a dot. The wavy line is a gluon.

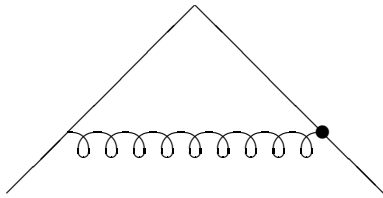
symbolically represents the sum of 12 different diagrams. They are all shown in Figs. 3.1 to 3.12, where the improved quark-gluon vertex (33) is represented by a dot and the insertion of $O(a)$ and $O(a^2)$ corrections to the vertex operators (see also eqs. (50) and (73)) are respectively indicated by an open circle and a square.



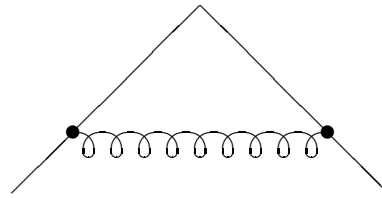
3.1



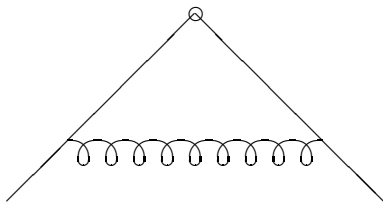
3.2



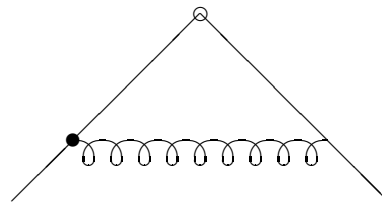
3.3



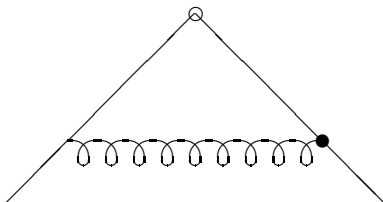
3.4



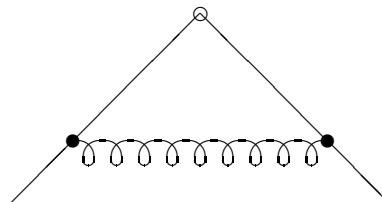
3.5



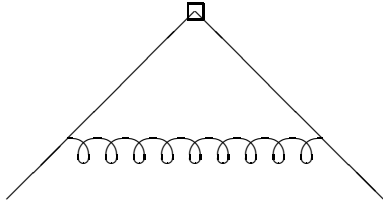
3.6



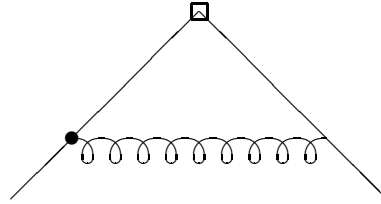
3.7



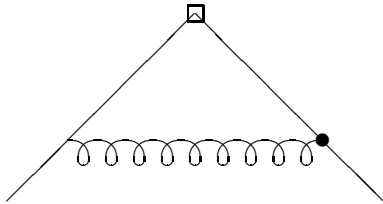
3.8



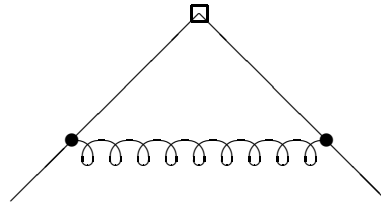
3.9



3.10



3.11



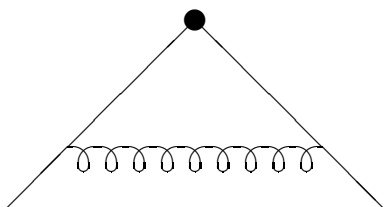
3.12

Fig. 3 - The 12 diagrams that contribute to the graph of Fig. 2. We have indicated the improved quark-gluon vertex with a dot and the insertions of $O(a)$ and $O(a^2)$ corrections to the vertex operators with respectively an open circle and a square.

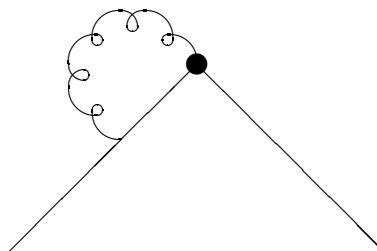
With this understanding we show below only the general patterns of the various graphs, as representatives of the full set of improved diagrams.

The graphs needed for the 1-loop computation of the matrix element $\langle q | (O_{\mu\nu}^q)^{IMPR} | q \rangle$ and the graphs contributing in the quenched approximation to $\langle g, \sigma | O_{\mu\nu}^g | g, \sigma \rangle$ are shown in Figs. 4.1 to 4.8 and Figs. 5.1 to 5.13 respectively, where the insertion of the vertex operator is always indicated

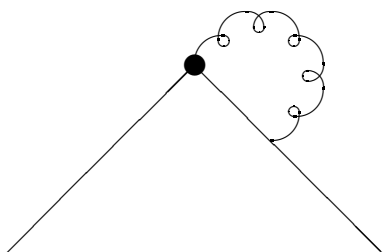
by a dot.



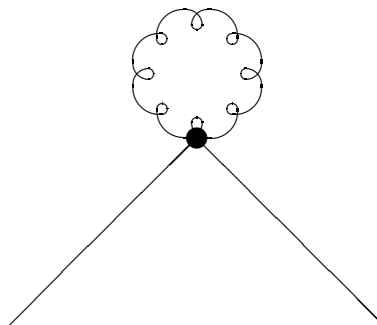
4.1 - Vertex



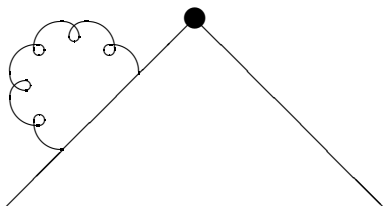
4.2 - Sail



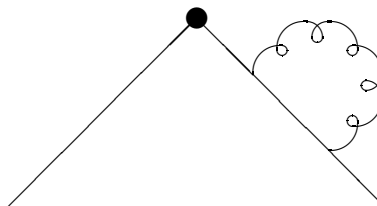
4.3 - Sail



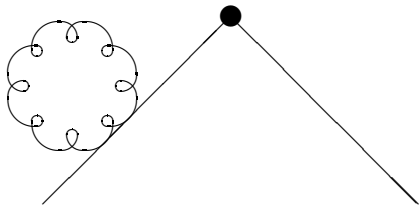
4.4 - Operator tadpole



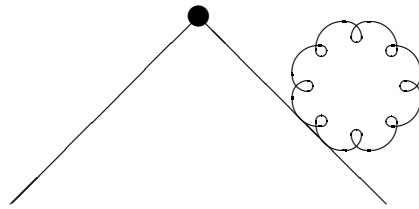
4.5 - Self-energy



4.6 - Self-energy

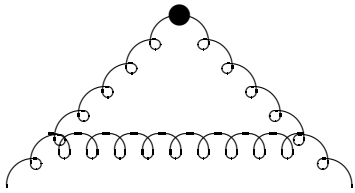


4.7 - Leg tadpole

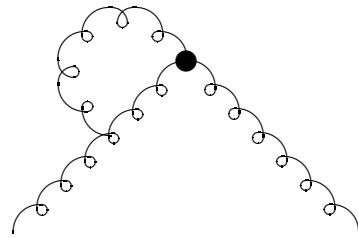


4.8 - Leg tadpole

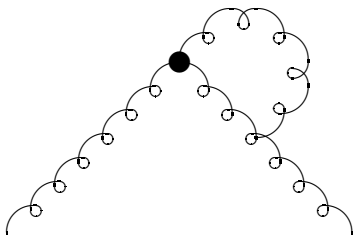
Fig. 4 - The different types of graphs contributing to the 1-loop approximation of the matrix element $\langle q | (O_{\mu\nu}^q)^{IMPR} | q \rangle$.



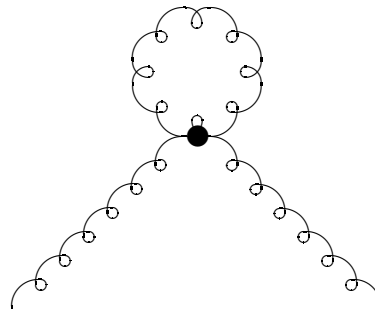
5.1 - Vertex



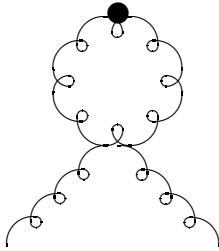
5.2 - Sail



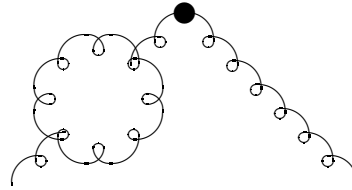
5.3 - Sail



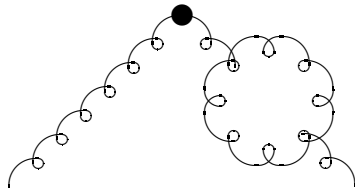
5.4 - Operator tadpole



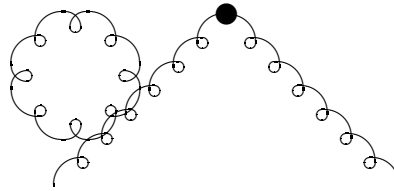
5.5 - Tadpole (QCD vertex)



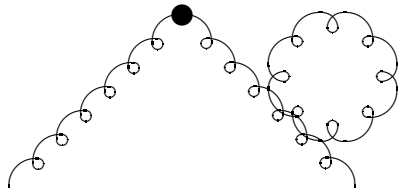
5.6 - Gluon loop



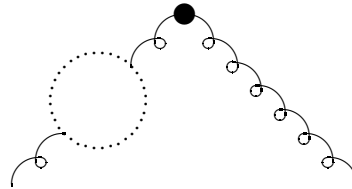
5.7 - Gluon loop



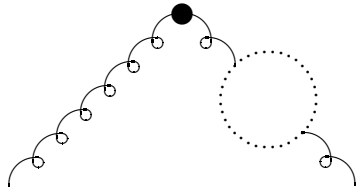
5.8 - Leg tadpole



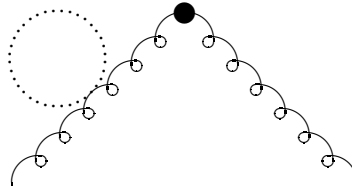
5.9 - Leg tadpole



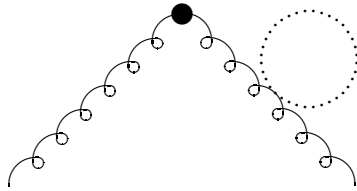
5.10 - Ghost



5.11 - Ghost

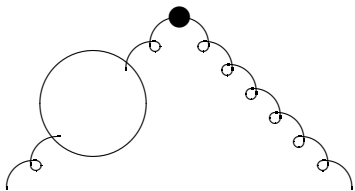


5.12 - Ghost

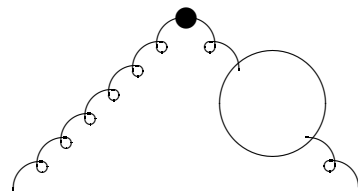


5.13 - Ghost

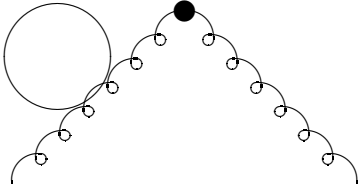
Fig. 5 - The different types of graphs contributing to the 1-loop approximation of the matrix element $\langle g, \sigma | O_{\mu\nu}^g | g, \sigma \rangle$, in the quenched approximation. The dotted line represents a ghost loop.



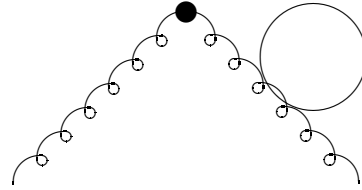
6.1 - Quark loop



6.2 - Quark loop



6.3 - Tadpole-quark loop



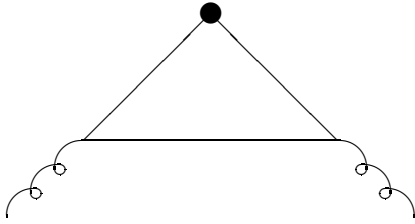
6.4 - Tadpole-quark loop

Fig. 6 - The different types of graphs contributing to the 1-loop approximation of the matrix element $\langle g, \sigma | O_{\mu\nu}^g | g, \sigma \rangle$ to be added in the full (unquenched) theory to the diagrams of Figs. 5.

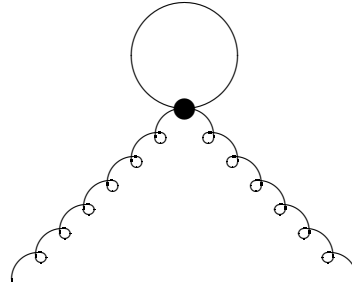
In the full (unquenched) theory there will be mixing between the flavor Singlet operators $(O_{\mu\nu}^q)^{IMPR}$ and $O_{\mu\nu}^g$. To compute the mixing coefficients we have

1) to add to the diagrams of Figs. 5 those of Figs. 6, in which a quark loop is present.

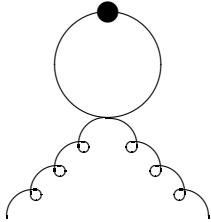
2) to evaluate the off-diagonal matrix elements $\langle g, \sigma | (O_{\mu\nu}^q)^{IMPR} | g, \sigma \rangle$ and $\langle q | O_{\mu\nu}^g | q \rangle$. The corresponding diagrams are listed in Figs. 7 and Figs. 8 respectively.



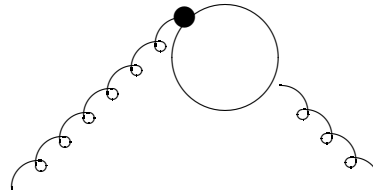
7.1



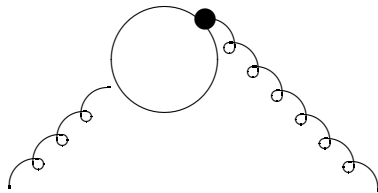
7.2



7.3

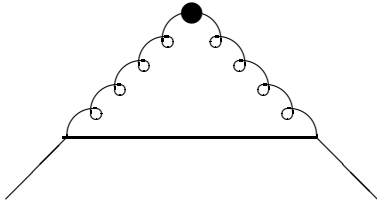


7.4

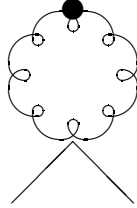


7.5

Fig. 7 - The different types of graphs contributing to the 1-loop approximation of the matrix element $\langle g, \sigma | (O_{\mu\nu}^q)^{IMPR} | g, \sigma \rangle$.



8.1



8.2

Fig. 8 - The different types of graphs contributing to the 1-loop approximation of the matrix element $\langle q|O_{\mu\nu}^g|q \rangle$.

Appendix C

Products of sines

At some intermediate stage of the computation there appear expressions whose general structure is of the kind

$$\mathcal{I}(\mu_1, \dots, \mu_{2n}) = \int d^4k f(\cos k, \sum_{\lambda} \sin^2 k_{\lambda}) \prod_{i=1}^{2n} \sin k_{\mu_i}, \quad (77)$$

By exploiting the H(4) covariance properties of the integrand, the integral (77) is first reduced to a sum of simpler terms that have the form

$$\int d^4k f(\cos k, \sum_{\lambda} \sin^2 k_{\lambda}) \prod_{\mu=1}^4 \sin^{2n_{\mu}} k_{\mu}, \quad (78)$$

where n_{μ} are integers ranging between 0 and n and satisfying

$$\sum_{\mu=1}^4 n_{\mu} = n. \quad (79)$$

For example in the $n = 2$ case one gets

$$\begin{aligned}
\mathcal{I}(\mu_1, \mu_2, \mu_3, \mu_4) &= \int d^4k f(\cos k, \sum_{\lambda} \sin^2 k_{\lambda}) \sin k_{\mu_1} \sin k_{\mu_2} \sin k_{\mu_3} \sin k_{\mu_4} = \\
&\int d^4k f(\cos k, \sum_{\lambda} \sin^2 k_{\lambda}) \sin^2 k_{\mu_1} \sin^2 k_{\mu_3} \delta_{\mu_1\mu_2} \delta_{\mu_3\mu_4} \Big|_{\mu_1 \neq \mu_3} \\
&+ \int d^4k f(\cos k, \sum_{\lambda} \sin^2 k_{\lambda}) \sin^2 k_{\mu_1} \sin^2 k_{\mu_2} \delta_{\mu_1\mu_3} \delta_{\mu_2\mu_4} \Big|_{\mu_1 \neq \mu_2} \\
&+ \int d^4k f(\cos k, \sum_{\lambda} \sin^2 k_{\lambda}) \sin^2 k_{\mu_1} \sin^2 k_{\mu_2} \delta_{\mu_1\mu_4} \delta_{\mu_2\mu_3} \Big|_{\mu_1 \neq \mu_2} \\
&\quad + \int d^4k f(\cos k, \sum_{\lambda} \sin^2 k_{\lambda}) \sin^4 k_{\mu_1} \delta_{\mu_1\mu_2\mu_3\mu_4}, \tag{80}
\end{aligned}$$

where $\delta_{\mu_1\mu_2\mu_3\mu_4}$ is non-zero only if all the indices are equal.

In the form (80) this equation is not suited for the further algebraic manipulations that Schoonschip will have to perform. To overcome this problem we have simply to implement algebraically the various conditions $\mu_i \neq \mu_j$ in eq. (80) by writing

$$\sin^2 k_{\mu_1} \sin^2 k_{\mu_2} \Big|_{\mu_1 \neq \mu_2} = \sin^2 k_{\mu_1} \sin^2 k_{\mu_2} - \sin^4 k_{\mu_1} \delta_{\mu_1\mu_2} \tag{81}$$

and the like. This leads to the formula

$$\begin{aligned}
\mathcal{I}(\mu_1, \mu_2, \mu_3, \mu_4) &= \int d^4k f(\cos k, \sum_{\lambda} \sin^2 k_{\lambda}) \sin k_{\mu_1} \sin k_{\mu_2} \sin k_{\mu_3} \sin k_{\mu_4} = \\
&\int d^4k f(\cos k, \sum_{\lambda} \sin^2 k_{\lambda}) \sin^2 k_{\mu_1} \sin^2 k_{\mu_3} \delta_{\mu_1\mu_2} \delta_{\mu_3\mu_4} \\
&+ \int d^4k f(\cos k, \sum_{\lambda} \sin^2 k_{\lambda}) \sin^2 k_{\mu_1} \sin^2 k_{\mu_2} \delta_{\mu_1\mu_3} \delta_{\mu_2\mu_4} \\
&+ \int d^4k f(\cos k, \sum_{\lambda} \sin^2 k_{\lambda}) \sin^2 k_{\mu_1} \sin^2 k_{\mu_2} \delta_{\mu_1\mu_4} \delta_{\mu_2\mu_3} \\
&\quad - 2 \cdot \int d^4k f(\cos k, \sum_{\lambda} \sin^2 k_{\lambda}) \sin^4 k_{\mu_1} \delta_{\mu_1\mu_2\mu_3\mu_4}. \tag{82}
\end{aligned}$$

If n is higher, the way to get useful expressions is the same, but it is necessary to use relations of the kind (81) several times. The expansions for n up to 4 are summarized in Tables C.1 to C.3.

Type of term	Number of permutations	Weight of each permutation
" $\delta_{\mu_1\mu_2}\delta_{\mu_3\mu_4}$ "	3	1
" $\delta_{\mu_1\mu_2\mu_3\mu_4}$ "	1	-2

Table C.1 - Numerical coefficients for the expansion of $\mathcal{I}(\mu_1, \mu_2, \mu_3, \mu_4)$

Type of term	Number of permutations	Weight of each permutation
" $\delta_{\mu_1\mu_2}\delta_{\mu_3\mu_4}\delta_{\mu_5\mu_6}$ "	15	1
" $\delta_{\mu_1\mu_2}\delta_{\mu_3\mu_4\mu_5\mu_6}$ "	15	-2
" $\delta_{\mu_1\mu_2\mu_3\mu_4\mu_5\mu_6}$ "	1	16

Table C.2 - Numerical coefficients for the expansion of $\mathcal{I}(\mu_1, \mu_2, \mu_3, \mu_4, \mu_5, \mu_6)$

Type of term	Number of permutations	Weight of each permutation
" $\delta_{\mu_1\mu_2}\delta_{\mu_3\mu_4}\delta_{\mu_5\mu_6}\delta_{\mu_7\mu_8}$ "	105	1
" $\delta_{\mu_1\mu_2}\delta_{\mu_3\mu_4}\delta_{\mu_5\mu_6\mu_7\mu_8}$ "	210	-2
" $\delta_{\mu_1\mu_2}\delta_{\mu_3\mu_4\mu_5\mu_6\mu_7\mu_8}$ "	28	16
" $\delta_{\mu_1\mu_2\mu_3\mu_4}\delta_{\mu_5\mu_6\mu_7\mu_8}$ "	35	4
" $\delta_{\mu_1\mu_2\mu_3\mu_4\mu_5\mu_6\mu_7\mu_8}$ "	1	-272

Table C.3 - Numerical coefficients for the expansion of

$$\mathcal{I}(\mu_1, \mu_2, \mu_3, \mu_4, \mu_5, \mu_6, \mu_7, \mu_8)$$

A check on the correctness of these coefficients may be obtained by considering the case in which in eq. (77) all indices are equal. In this case there is only one contribution. This means that in each Table, if we sum the numbers obtained by multiplying the weight of each permutation by the number of permutations, we must get 1, as it is immediately checked in all cases.

Appendix D

α -integration

To reduce the computing time in the numerical integration of the integrals that involve fermion propagators, we have chosen to perform analytically the integration over the Feynman parameter α , and to leave for the numerical integration only a four-dimensional expression. To this end we need to compute integrals of the form

$$\mathbf{F}_{nm}(f(k), g(k)) = \int_0^1 d\alpha \frac{\alpha^n}{[f(k) + \alpha g(k)]^m}. \quad (83)$$

In our calculations we explicitly have

$$\begin{aligned} g(k) &= 4 \sum_{\lambda} \sin^2 \frac{k_{\lambda}}{2} - \left[\sum_{\lambda} \sin^2 k_{\lambda} + 4r^2 \left(\sum_{\lambda} \sin^2 \frac{k_{\lambda}}{2} \right)^2 \right] \\ f(k) &= \left[\sum_{\lambda} \sin^2 k_{\lambda} + 4r^2 \left(\sum_{\lambda} \sin^2 \frac{k_{\lambda}}{2} \right)^2 \right]. \end{aligned} \quad (84)$$

The functions \mathbf{F}_{nm} satisfy the recurrence relations

$$\frac{\partial}{\partial f} \mathbf{F}_{nm} = -m \cdot \mathbf{F}_{n \ m+1} \quad (85)$$

$$\frac{\partial}{\partial g} \mathbf{F}_{nm} = -m \cdot \mathbf{F}_{n+1 \ m+1} \quad (86)$$

which make simpler their computation and allow for a check of the formulae given below.

The formulae needed in this work are:

$$\begin{aligned}
F_{02} &= \frac{1}{f \cdot (g + f)} \\
F_{12} &= \frac{1}{g} \cdot \left[\frac{1}{g} \log \left(1 + \frac{g}{f} \right) - \frac{1}{g + f} \right] \\
F_{22} &= \frac{1}{g^2} \cdot \left[1 - 2 \frac{f}{g} \log \left(1 + \frac{g}{f} \right) + \frac{f}{g + f} \right] \\
F_{32} &= \frac{1}{g^2} \cdot \left[\frac{1}{2} - 2 \frac{f}{g} + 3 \frac{f^2}{g^2} \log \left(1 + \frac{g}{f} \right) - \frac{f^2}{g \cdot (g + f)} \right] \\
F_{03} &= \frac{g + 2f}{2f^2 \cdot (g + f)^2} \\
F_{13} &= \frac{1}{2f \cdot (g + f)^2} \\
F_{23} &= \frac{1}{g^2} \cdot \left[\frac{1}{g} \log \left(1 + \frac{g}{f} \right) - \frac{3g + 2f}{2 \cdot (g + f)^2} \right] \\
F_{33} &= \frac{1}{g^3} \cdot \left[1 - 3 \frac{f}{g} \log \left(1 + \frac{g}{f} \right) + f \frac{5g + 4f}{2 \cdot (g + f)^2} \right] \\
F_{43} &= \frac{1}{g^3} \cdot \left[\frac{1}{2} - 3 \frac{f}{g} + 6 \frac{f^2}{g^2} \log \left(1 + \frac{g}{f} \right) - f^2 \frac{7g + 6f}{2g \cdot (g + f)^2} \right] \\
F_{53} &= \frac{1}{g^3} \cdot \left[\frac{1}{3} - \frac{3f}{2g} + 6 \frac{f^2}{g^2} - 10 \frac{f^3}{g^3} \log \left(1 + \frac{g}{f} \right) + f^3 \frac{9g + 8f}{2g^2 \cdot (g + f)^2} \right] \\
F_{04} &= \frac{g^2 + 3gf + 3f^2}{3f^3 \cdot (g + f)^3} \\
F_{14} &= \frac{g + 3f}{6f^2 \cdot (g + f)^3} \\
F_{24} &= \frac{1}{3f \cdot (g + f)^3} \\
F_{34} &= \frac{1}{g^3} \cdot \left[\frac{1}{g} \log \left(1 + \frac{g}{f} \right) - \frac{11g^2 + 15gf + 6f^2}{6 \cdot (g + f)^3} \right].
\end{aligned} \tag{87}$$

References

- [1] G.Altarelli, Phys. Rep. **81** (1982) 1
- [2] J.D.Bjorken and E.A.Paschos, Phys. Rev. **185** (1969) 1975
- [3] R.P.Feynman, Phys. Rev. Lett. **23** (1969) 1415
- [4] D.J.Gross and F.Wilczek, Phys. Rev. Lett. **30** (1973) 1343
- [5] H.D.Politzer, Phys. Rev. Lett. **30** (1973) 1346
- [6] H.Fritzsch, M.Gell-Mann and H.Leutwyler, Phys. Lett. **B47** (1973) 365
- [7] B.Sheikholeslami and R.Wohlert, Nucl. Phys. **B259** (1985) 572
- [8] G.Heatlie, G.Martinelli, C.Pittori, G.C.Rossi and C.T.Sachrajda, Nucl. Phys. **B352** (1991) 266 and Nucl. Phys. **B** (Proc. Suppl.) **17** (1990) 607; E.Gabrielli, G.Heatlie, G.Martinelli, C.Pittori, G.C.Rossi, C.T.Sachrajda and A.Vladikas, Nucl. Phys. **B** (Proc. Suppl.) **20** (1991) 448
- [9] E.Gabrielli, G.Martinelli, C.Pittori, G.Heatlie and C.T.Sachrajda, Nucl. Phys. **B362** (1991) 475
- [10] R.Frezzotti, E.Gabrielli, C.Pittori and G.C.Rossi, Nucl. Phys. **B373** (1992) 781
- [11] G.Beccarini, S.Capitani and G.C.Rossi, in preparation
- [12] A.S.Kronfeld and D.M.Photiadis, Phys. Rev **D31** (1985) 2939
- [13] G.Martinelli and C.T.Sachrajda, Phys. Lett. **B196** (1987) 184 and Nucl. Phys. **B306** (1988) 865

- [14] G.Martinelli and C.T.Sachrajda, Nucl. Phys. **B316** (1989) 355
- [15] G.Corbò, E.Franco and G.C.Rossi, Phys. Lett. **B221** (1989) 367 and Phys. Lett. **B236** (1990) 196
- [16] S.Caracciolo, G.Curci, P.Menotti and A.Pelissetto, Phys. Lett. **B228** (1989) 375 and Annals of Physics **197** (1990) 119
- [17] S.Caracciolo, P.Menotti and A.Pelissetto, Nucl. Phys. **B375** (1992) 195
- [18] K.Symanzik, in “Mathematical Problems in Theoretical Physics”, Springer Lecture Notes in Physics, vol. **153** (1982) 47 (R.Schrader, R.Seiler and D.A.Uhlenbrock eds.)
- [19] G.Martinelli, C.T.Sachrajda, G.Salina and A.Vladikas, Nucl. Phys. **B378** (1992) 592; E: Nucl. Phys. **B397** (1993) 479
- [20] G.Martinelli, S.Petrarca, C.T.Sachrajda and A.Vladikas, Phys. Lett. **B311** (1993) 241
- [21] K.G.Wilson, Phys. Rev. **179** (1969) 1499
- [22] D.J.Gross and S.B.Treiman, Phys. Rev. **D4** (1971) 1059
- [23] D.J.Gross, in “Methods in field theory”, Les Houches, Session XXVIII, 1975, North-Holland (1976) 141 (R.Balian and J.Zinn-Justin eds.)
- [24] D.J.Gross and F.Wilczek, Phys. Rev. **D8** (1973) 3633 and Phys. Rev. **D9** (1974) 980
- [25] H.Georgi and H.D.Politzer, Phys. Rev. **D9** (1974) 416
- [26] W.A.Bardeen, A.J.Buras, D.W.Duke and T.Muta, Phys. Rev. **D18** (1978) 3998

- [27] N.Christ, B.Hasslacher and A.Mueller, Phys. Rev. **D6** (1972) 3543
- [28] M.Lüscher and P.Weisz, Commun. Math. Phys. **97** (1985) 59
- [29] K.G.Wilson, Phys. Rev. **D10** (1974) 2445 and in “New Phenomena in Subnuclear Physics”, Plenum Press, New York (1977) (A.Zichichi ed.)
- [30] H.W.Hamber and C.M.Wu, Phys. Lett. **B133** (1983) 351 and Phys. Lett. **B136** (1984) 255
- [31] W.Wetzel, Phys. Lett. **B136** (1984) 407
- [32] T.Eguchi and N.Kawamoto, Nucl. Phys. **B237** (1984) 609
- [33] M.P.Lombardo, G.Parisi and A.Vladikas, Nucl. Phys. **B395** (1993) 388
- [34] S.Naik, Phys. Lett. **B311** (1993) 230
- [35] A.X. El-Khadra, G.Hockney, A.S.Kronfeld and P.B.Mackenzie, Phys. Rev. Lett. **69** (1992) 729
- [36] A.X. El-Khadra, Nucl. Phys. **B** (Proc. Suppl.) **30** (1993) 449
- [37] M.Baake, B.Gemünden and R.Oedingen, Journ. Math. Phys. **23** (1982) 944
- [38] J.Mandula, G.Zweig and J.Govaerts, Nucl. Phys. **B228** (1983) 91
- [39] M.Bochicchio, L.Maiani, G.Martinelli, G.C.Rossi and M.Testa, Nucl. Phys. **B262** (1985) 445
- [40] A.Borrelli, C.Pittori, R.Frezzotti and E.Gabrielli, Nucl. Phys. **B409** (1993) 382
- [41] H.Kawai, R.Nakayama and K.Seo, Nucl. Phys. **B189** (1981) 40

- [42] G.Parisi, in “High Energy Physics-1980”, proceedings of the XX International Conference, Madison, Wisconsin, American Institute of Physics (1981) (L.Durand and L.G.Pondrom eds.)
- [43] A.Hasenfratz and P.Hasenfratz, Phys. Lett. **B93** (1980) 165
- [44] G.P.Lepage, Nucl. Phys. **B** (Proc. Suppl.) **26** (1992) 45; G.P.Lepage and P.B.Mackenzie, Phys. Rev. **D48** (1993) 2250; G.P.Lepage, Lattice QCD for small computers, Lectures presented at TASI 93 (Boulder, June 1993) and at the UK Summer Institute (St. Andrews, Aug 1993)
- [45] G.Martinelli, private communication
- [46] G.Curci, E.Franco, L.Maiani and G.Martinelli, Phys. Lett. **B202** (1988) 363
- [47] S.Capitani, J.P.Leroy, J.Micheli, C.Pittori and G.C.Rossi, work in progress
- [48] G.Martinelli, M.Paciello, S.Petrarca, C.Pittori, C.T.Sachrajda, B.Taglienti, M.Testa and A.Vladikas, University of Southampton Preprint SHEP 93-94-04 (Dec 1993)